J. Fluid Mech. (1981), *vol.* 107, *pp.* 339–373
Printed in Great Britain

Wall effect on the bubble behaviour in highly viscous liquids

By MADELEINE COUTANCEAU
AND PATRICK THIZON

Laboratoire de Mécanique des Fluides, Université de Poitiers, France

(Received 8 February 1979 and in revised form 11 December 1979)

A theoretical and experimental study is carried out for the problem of the wall effect experienced by a fluid body moving with a constant speed along the axis of a vertical circular tube filled with a highly viscous liquid. In the theoretical study the body is limited to being either spherical or cylindrical and an optimization process with least squares is used to write the no-slip condition on the tube wall. Comparisons between the hydrodynamic and kinematic behaviour of a rigid, liquid and gaseous body are established. Furthermore, from an experimental investigation, based upon a fine visualization technique and rising-speed measurements, the respective limits of validity of the calculations have been found in the case of an air bubble. Information concerned especially with the shape of this bubble, and the hydrodynamic field that it generates, is given for the whole domain of the bubble and tube diameter ratio ranging from no wall influence to maximum wall influence.

1. Introduction

Drops and bubbles in fluids play an important part in numerous industrial processes and consequently a great deal of theoretical and experimental work has been done in this field, see, for example, Gal-Or, Klinzing & Tavlarides (1969), Harper (1972), Grace (1973), Wallis (1974), Grace, Wairegi & Nguyen (1976) and Van Wijngaarden & Vossers' (1978) recent report on the Euromech Colloquium 98 concerned with gas bubbles in liquids.

From these investigations, it appears that there is a particular shortage of data concerning drops and bubbles suspended in very highly viscous liquids, even though this phenomenon is illustrated in many applications: some techniques of extraction and transportation of oil products; glass bubbling and fluidization; etc. On the other hand, it is found that the wall effect is rarely taken into account, although the drops or bubble behaviours, as well as the hydrodynamic field they generate, may be appreciably influenced by the container even when the wall is not in the near vicinity.

Consequently in this present work we consider as a basic investigation the problem of a single bubble† rising along the axis of a vertical circular tube filled with a quiescent liquid of high viscosity. In these conditions, the viscosity effects are dominant compared with inertia and surface-tension effects; this regime is often called the 'Hadamard regime'. Thus, in an unbounded medium, the shape of the bubble would be a sphere and its terminal speed would be given by the Hadamard (1911) or Rybczyński

† The size of the bubble is assumed to be sufficient for an internal motion to develop so that the bubble behaves effectively as a fluid body and not as a solid body.

(1911) formula. This is still true when the tube diameter is very large with respect to the bubble diameter. However, as the tube diameter becomes smaller, the bubble behaviour is modified: the drag that is experienced becomes relatively greater and the bubble's shape becomes longer and, in a limiting case, nearly 'cylindrical'. Hence we have what is usually called a 'cylindrical bubble'.

It is important to know this wall effect. Nevertheless, such effects have been little studied particularly when they remain moderate and in the case of the Hadamard regime. Uno & Kintner (1956) proposed an empirical velocity correction factor in terms of the bubble and tube diameter ratio and of the surface tension of the liquid, but the fluids tested experimentally were of relatively low viscosity ($\mu < 0{\cdot}25$ P) and then the regime was different (for example, the shapes of the bubbles were oblate ellipsoids, with axes perpendicular to the tube axis, and not spheres or prolate ellipsoids as they would be in the Hadamard regime). From a theoretical point of view, Haberman & Sayre (1958) assumed that the drop or bubble retained a spherical shape and they gave a first approximation of the corresponding creeping flow (some experimental results were also presented for a drop). Satapathy & Smith (1961) substituted the cylindrical boundary with a spherical one, coaxial with the bubble and tangential to the tube in the equatorial plane. Collins (1967) examined the wall effect induced by a tube in the case of large spherical cap bubbles rising in a perfect suspending liquid. Hetsroni, Haber & Wacholder (1970) and Ho & Leal (1975) considered drops moving axially in a Poiseuille flow: the former from a theoretical point of view, the latter experimentally. Cylindrical drops and bubbles have been more extensively studied: Dumitrescu (1943), Davies & Taylor (1950), Nicklin, Wilkes & Davidson (1962) and Tung & Parlange (1976) considered the case of long air bubbles or 'slugs' in water or in low-viscosity liquids and did not take viscosity into account. On the other hand, Goldsmith & Mason (1962, 1963), White & Beardmore (1962) and Zukoski (1966) presented useful results in the case of bubbles in a viscous liquid.

No one seems to have examined the problem for the whole domain ranging from no wall influence to maximum wall influence (cylindrical bubble); it appears to us well worth investigating.

2. Dimensional analysis

In order to draw a comparison between the behaviour of drops and bubbles moving through different fluids, it is necessary to make a dimensional investigation. Here we suppose that the two adjacent fluids are Newtonian, incompressible and isothermal. In this case, an analysis of the phenomena shows that the terminal velocity U_0 of the bubble is a function of the gravitational acceleration g, the dynamic viscosities μ_e and μ_i, the densities ρ_e and ρ_i of the external and internal phases, the surface tension σ, the equivalent diameter d_e (i.e. the diameter of the sphere having the same volume as the drop or bubble) and the distance L to the wall. Because $\Delta\rho = \rho_e - \rho_i$ plays a dominant part in the motion of the suspended phase, it is often considered instead of ρ_i, and we can therefore write

$$f_1(U_0, g, \rho_e, \mu_e, \mu_i, \Delta\rho, \sigma, d_e, L) = 0. \tag{2.1}$$

From the Waschy–Buckingham theorem, it is possible to simplify the investigation by grouping these nine parameters in only six dimensionless groups without losing

any information. If (as in the case of solid bodies) U_0, d_e, ρ_e are chosen for the normalization of the other parameters contained in the relation (2.1), these dimensionless groups are found to be:

$$Re = \frac{U_0 d_e \rho_e}{\mu_e}, \quad Fr = \frac{U_0^2 \rho_e}{\Delta\rho g d_e}, \quad We = \frac{\rho_e U_0^2 d_e}{\sigma}, \quad \frac{\mu_i}{\mu_e}, \quad \frac{\Delta\rho}{\rho_e}, \quad \frac{d_e}{L}, \tag{2.2}$$

and, putting $\lambda = d_e/L$, equation (2.1) becomes

$$f_2\left(Re, Fr, We, \frac{\mu_i}{\mu_e}, \frac{\Delta\rho}{\rho_e}, \lambda\right) = 0. \tag{2.3}$$

The Reynolds number Re, the Froude number Fr and the Weber number We characterize the importance of the inertial forces in comparison with the viscosity forces, the gravitational forces and the interfacial forces respectively. However, this formulation does not appear to be very appropriate because the terminal speed U_0 of the drop, which is usually one of the unknown variables of the problem, is contained in all of the three groups: Re, Fr We. A more convenient set of dimensionless groups can be obtained from the measurable physical properties of the suspending fluid (ρ_e and μ_e) with, in addition, the gravitational acceleration g instead of U_0, d_e, ρ_e. Thus new groups appear such as the dimensionless velocity U_0^* and diameter d_e^*,

$$U_0^* = U_0\left(\frac{\rho_e^2}{\mu_e g \Delta\rho}\right)^{\frac{1}{3}}, \quad d_e^* = d_e\left(\frac{\rho_e g \Delta\rho}{\mu_e^2}\right)^{\frac{1}{3}}, \tag{2.4}$$

and the property group

$$Po = \left(\frac{\sigma^3 \rho_e^2}{\mu_e^4 g \Delta\rho}\right)^{\frac{1}{3}} \tag{2.5}$$

which contains only the physical properties of the phases. So equation (2.1) can be written as

$$f_3\left(U_0^*, d_e^*, Po, \frac{\mu_i}{\mu_e}, \frac{\Delta\rho}{\rho_e}, \lambda\right) = 0. \tag{2.6}\dagger$$

Another suitable set of groups is also often used: they are the Reynolds number Re, the Etvös number Eo ($= \Delta\rho g d_e^2/\sigma$) representing the ratio between the gravitational and the interfacial forces and the Morton number Mo($= Po^{-3}$), so we have

$$f_4\left(Re, Eo, Mo, \frac{\mu_i}{\mu_e}, \frac{\Delta\rho}{\rho_e}, \lambda\right) = 0. \tag{2.7}$$

It is to be remarked that the various sets of non-dimensional groups introduced in this analysis are not independent, so for example

$$Re = U_0^* d_e^*, \quad Eo = d_e^{*2} Po^{-1}, \quad Mo = Po^{-3} = We^3 Fr^{-1} Re^{-4}.$$

On the other hand, in the case of gas bubbles suspended in liquids the ratio $\Delta\rho/\rho_e$ may be taken as unity and the viscosity ratio μ_i/μ_e tends towards zero and therefore loses any importance. Thus, the general equations (2.3), (2.6), (2.7) are simplified; for example the last is reduced to

$$f_5(Re, Eo, Mo, \lambda) = 0. \tag{2.8}$$

† The group U_0^*, d_e^*, $P = Po^3$ was also proposed by Wallis (1974) in his synthesis work concerned with drops and bubbles in an infinite medium.

Furthermore, when one or more of the retarding forces are negligible compared with the others, a lesser number of groups is sufficient to represent the phenomenon provided they are suitably chosen. For instance, as White & Beardmore (1962) mentioned, when the inertial forces are negligible, the Poiseuille number Ps ($Ps = U_0\mu_e/\Delta\rho g d_e^2 = Fr/Re$), representing the relative importance of the viscous and gravitational forces, may be considered as the group involving U_0, and in addition, when the interfacial forces are negligible, no other group is required other than λ.

3. Theoretical study

As limiting cases we consider successively a spherical and a cylindrical single drop G† with a radius R (for the sphere) or R_E (for the cylinder) in a uniform rectilinear motion with the speed U_0, along the axis of a vertical and infinitely long circular tube T. This tube, of radius R_T, is filled with a liquid which lies at rest away from the drop. We assume that the two fluids are incompressible, isothermal and Newtonian and that the Reynolds numbers Re_e and Re_i of the corresponding flows, exterior (E_e) and interior (E_i) to G, are sufficiently low so that the flows are creeping and the Stokes simplification is justified. The surface-tension effects are also neglected. The motion is referred to a frame which is fixed to the drop and whose polar axis **z** coincides with the tube one. So, in this frame, the drop appears to be at rest, whereas the tube and the fluid in a far-away cross-section are moving with the velocity U_0.

All the quantities are non-dimensionalized by choosing as reference units: the speed U_0, the radius R (or R_E), the density ρ_e of the external fluid. So here, for a simple formulation of the problem, the following parameters are introduced:

$$\lambda = \frac{R}{R_T}, \quad \omega = \frac{\mu_e}{\mu_i}, \quad Ps = \frac{\mu_e U_0}{4\Delta\rho g R^2}.$$

Considering the hypotheses proposed, the equations to be satisfied by the velocity fields of E_e and E_i are

$$\operatorname{curl}^3 U = 0, \quad \operatorname{div} U = 0. \tag{3.1), (3.2}$$

The boundary conditions can be specified as follows:

(i) No slip on the tube wall.

(ii) Uniform (equal to unit) velocity distribution far away from G.

(iii) At the drop surface: (*a*) continuity of the tangential velocity components; (*b*) cancellation of the normal velocity components; (*c*) continuity of the tangential components of the stress; (*d*) continuity of the normal components of the stress.

3.1. *Case of the spherical drop*

3.1.1. *Formulation of the problem*

First, let us consider the case of the drop as a fluid sphere. Then for convenience the motion is referred to a spherical co-ordinate system r, θ, ϕ (figure 1*a*) that moves with the drop and whose origin is taken at its centre.

So the boundary conditions at the drop surface (iii) take the form:

$$\left.\begin{aligned} U_{\theta_e}(1,\theta) = U_{\theta_i}(1,\theta), \quad U_{r_e}(1,\theta) = 0, \quad U_{r_i}(1,\theta) = 0, \\ F_{r\theta_e}(1,\theta) = F_{r\theta_i}(1,\theta), \quad F_{rr_e}(1,\theta) = F_{rr_i}(1,\theta), \end{aligned}\right\} \tag{3.3}$$

† The air bubble will be one particular case of this theoretical investigation.

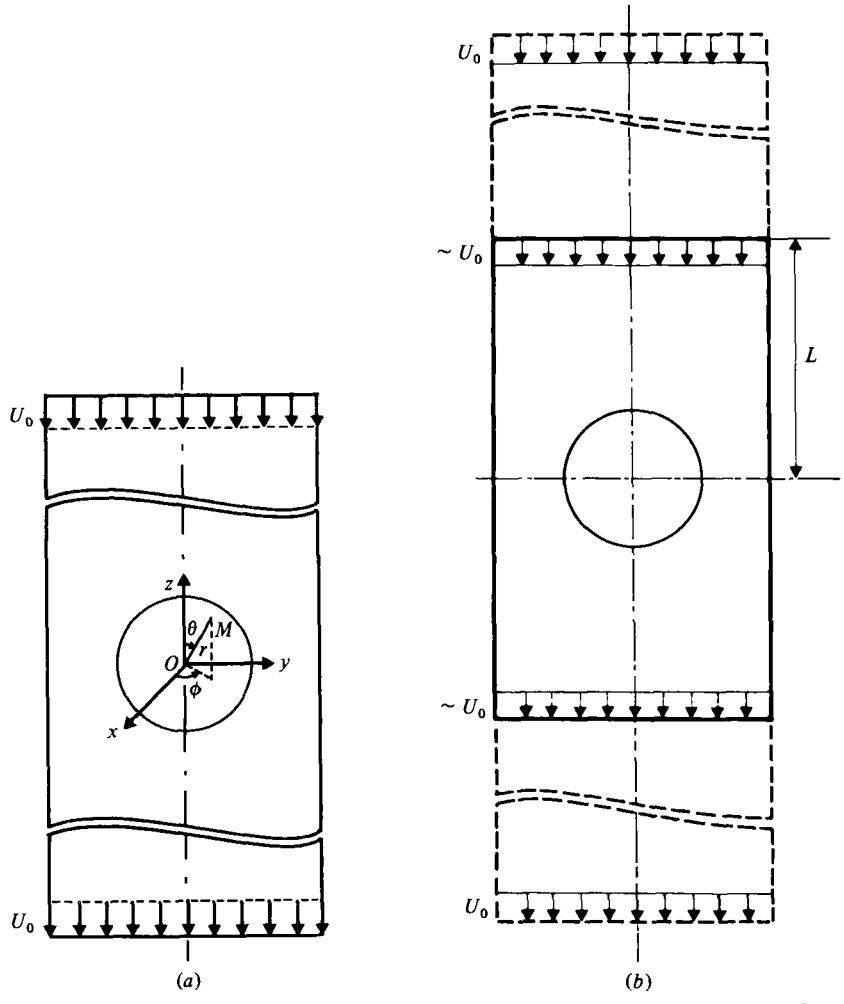

FIGURE 1. (*a*) Spherical reference co-ordinate frame. (*b*) Delimitation of the domain concerned in the calculation.

where U_r and U_θ stand for the radial and tangential components of the velocity field and F_{rr} and $F_{r\theta}$ for the radial and tangential components of the stress (including the one due to the pressure field); the indices e and i refer to quantities exterior to the fluid sphere and interior to it respectively.

On the other hand, the flow being axisymmetric and meridian ($U_\phi = 0$), the equation of continuity (3.2) involves the existence of a stream function $\psi(r, \theta)$ which is related to the velocity components by:

$$U_r = -\frac{1}{r^2}\frac{\partial \psi}{\partial t}, \quad U_\theta = -\frac{1}{rs}\frac{\partial \psi}{\partial r}, \tag{3.4}$$

with

$$t = \cos\theta \quad \text{and} \quad s = \sin\theta.$$

So that the motion equations (3.1) and (3.2) may be replaced by the equivalent one:

$$L^2 \psi(r, \theta) = 0, \tag{3.5}$$

where the differential operator L is defined by

$$L = \frac{\partial^2}{\partial r^2} + \frac{1-t^2}{r^2}\frac{\partial^2}{\partial t^2}.$$

A general solution of the equation (3.5) expressed in terms of products of r and t functions seems to have been proposed for the first time by Sampson (1891). In this case taking into account the symmetries of the two flows (E_e and E_i) and eliminating the terms involving singularities on the flow axis and at the origin, this solution gives respectively:

$$\psi_e = \sum_{n=2,4,\ldots}^{\infty} C_n^{-\frac{1}{2}}(t)\,[a_n r^{-n+1} + b_n r^{-n+3} + c_n r^n + d_n r^{n+2}], \tag{3.6}$$

$$\psi_i = \sum_{n=2,4,\ldots}^{\infty} C_n^{-\frac{1}{2}}(t)\,[e_n r^n + f_n r^{n+2}], \tag{3.7}$$

where a_n, b_n, c_n, d_n, e_n, f_n represent arbitrary coefficients to be determined by the boundary conditions and $C_n^{-\frac{1}{2}}(t)$ the Gegenbauer polynomial of degree n and order $-\frac{1}{2}$ which is related to the Legendre polynomial by

$$C_n^{-\frac{1}{2}}(t) = \int_{-1}^{t} P_{n-1}(t)\,dt = \frac{1}{2n-1}\,(P_n(t) - P_{n-2}(t)).$$

The corresponding expressions of the radial and tangential velocity components can be obtained by substituting expressions (3.6) and (3.7) in the relation (3.4) and, in turn, the radial and tangential components of the stress by substituting these velocity components in the Newton's constitutive equation; but for brevity they are not given here. Hence we can express the boundary conditions on the drop surface. These conditions involve certain relations between the arbitrary coefficients $a_n, \ldots, f_n$ of (3.6) and (3.7), and so we obtain

$$\left.\begin{aligned}
&(n-1)\,a_n + (n-3)\,b_n - nc_n - (n+2)\,d_n = -ne_n - (n+2)f_n,\\
&a_n + b_n + c_n + d_n = 0, \quad e_n + f_n = 0,\\
&(n^2-1)\,a_n + n(n-2)\,b_n + n(n-2)\,c_n + (n^2-1)\,d_n = \frac{1}{\omega}[n(n-2)\,e_n + (n^2-1)f_n],\\
&-(1+n)\,a_n - \frac{n^2+n-3}{n}\,b_n + (n-2)\,c_n + \frac{n^2-3n-1}{n-1}\,d_n\\
&\qquad = \frac{1}{\omega}\left[(n-2)\,e_n + \frac{n^2-3n-1}{n-1}f_n\right] - \left[\frac{1}{8Ps}\right]_{n=2},\ \dagger
\end{aligned}\right\} \tag{3.8}$$

for $n = 2, 4, \ldots, \infty$. Equation (3.8) verifies that the motion is governed only by the Poiseuille number, as we could expect, considering the hypotheses formulated. On the other hand, two other equations (obtainable from the boundary conditions (i) and (ii)), have to be added to the five equations of the system (3.8); we now have in fact, for each value of n, a set of seven equations for the determination of only six unknown coefficients. The extra equation arises because the shape of the bubble has been *a priori* fixed. But, the shape of the bubble results from the motion itself and should be determined by the last equation of the system (3.8). Up to now this complex problem does not seem to have been solved in this case; only Hetsroni *et al.* (1970) gave a first

† The symbol $[\ ]_{n-2}$ signifies that the corresponding term must be taken into account for $n = 2$ only.

approximation when a Poiseuille velocity variation is imposed far from the drop. However, we hope to be able to do it later using the numerical least-squares technique that we present in this paper; some calculations are being carried out in this direction.

For the present work, the drop shape being supposedly spherical, the last equation of the system (3.8) is dropped (except for $n = 2$). But, at the end of the calculation (when the coefficients will be determined numerically), we shall evaluate the difference between the two corresponding normal components of the stress (interior and exterior) so as to verify the validity of the hypotheses made. Indeed, though in the case of a drop the spherical shape is compatible only with an unbounded external medium or a medium limited by a spherical boundary, it will be verified that, if the first term ($n = 2$) of the series (3.6) and (3.7) is dominant, this spherical shape constitutes also a very good approximation for the drop within a tube. This will be also confirmed by experiment.

Now, considering the first four equations of the system (3.8), it is possible to express a_n, c_n, e_n, f_n in terms of b_n and d_n for instance, and so we obtain

$$\left.\begin{aligned} a_n &= -[2n-3)\,b_n + 2(\omega-1)\,d_n]/K, \\ c_n &= -[2(\omega+1)\,b_n + (2n+1)\,d_n]/K, \\ e_n &= -f_n = \omega[(2n-3)\,b_n - (2n+1)\,d_n]/K, \end{aligned}\right\} \tag{3.9}$$

where

$$K = 2\omega + 2n - 1.$$

For the particular value $n = 2$, taking into account the above relations (3.9), one can see that the last equation of the system (3.8), which is the only one to contain gravity (through Ps), gives:

$$Ps = \frac{1}{12b_2}. \tag{3.10}$$

This relation (3.10) expresses the balance between the buoyancy and the drag forces;† it provides the terminal speed of the drop at steady state when the volume of the drop and the physical properties of the fluids are known.

For the convenience (automatization and minimal storage) of numerical calculations using electronic computers, we write the velocity components in the following linear forms

$$\left.\begin{aligned} U_{r_e} &= -\sum_{j=1,2,\ldots}^{\infty} A_j FA_j(r,t), \quad U_{\theta_e} = \sum_{j=1,2,\ldots}^{\infty} A_j FB_j(r,t), \\ U_{r_i} &= -\sum_{j=1,2,\ldots}^{\infty} A_j FC_j(r,t), \quad U_{\theta_i} = \sum_{j=1,2,\ldots}^{\infty} A_j FD_j(r,t), \end{aligned}\right\} \tag{3.11}$$

putting

$$A_{2n-1} = b_{2n}, \quad A_{2n} = d_{2n},$$

† It is known (Happel & Brenner 1965; Coutanceau 1971) that the non-dimensional drag experienced by an arbitrary shaped body, moving with a constant velocity U_0, is given (for the creeping regime) by $4\pi b_2$ (b_2 being the coefficients of the expansion (3.6)); so, for a spherical body of radius R, the dimensional drag is $T = 4\pi\mu_e b_2 RU_0$ and the balance between the buoyancy and drag forces gives: $\frac{4}{3}\pi R^3 \Delta\rho g = 4\pi\mu_e b_2 RU_0$, so consequently $Ps = 1/12b_2$.

and

$$\left.\begin{aligned}
FA_{2n-1}(r,t) &= \left[\frac{P_{2n-1}(t)}{K'}\right][-(4n-3)\,r^{-1-2n}+K'r^{1-2n}-2(\omega+1)\,r^{2n-2}],\\
FA_{2n}(r,t) &= \left[\frac{P_{2n-1}(t)}{K'}\right][-2(\omega-1)\,r^{-1-2n}-(4n+1)\,r^{2n-2}+K'r^{2n}],\\
FB_{2n-1}(r,t) &= \left[\frac{C_{2n}(t)}{sK'}\right][-(2n-1)(4n-3)\,r^{-1-2n}\\
&\qquad +(2n-3)\,K'r^{1-2n}+4n(\omega+1)\,r^{2n-2}]\\
FB_{2n}(r,t) &= \left[\frac{C_{2n}(t)}{sK'}\right][-2(2n-1)(\omega-1)\,r^{-1-2n}\\
&\qquad +2n(4n+1)\,r^{2n-2}-(2n+2)\,K'r^{2n}]\\
FC_{2n-1}(r,t) &= \left[\frac{(4n-3)\,\omega P_{2n-1}(t)}{K'}\right][r^{2n-2}-r^{2n}],\\
FC_{2n}(r,t) &= -\left[\frac{(4n+1)\,\omega P_{2n-1}(t)}{K'}\right][r^{2n-2}-r^{2n}],\\
FD_{2n-1}(r,t) &= -\left[\frac{(4n-3)\,\omega C_{2n}(t)}{sK'}\right][2nr^{2n-2}-(2n+2)\,r^{2n}],\\
FD_{2n}(r,t) &= \left[\frac{(4n+1)\,\omega C_{2n}(t)}{sK'}\right][2nr^{2n-2}-(2n+2)\,r^{2n}],
\end{aligned}\right\} \tag{3.12}$$

for $n = 1, 2, \ldots, \infty$ and where

$$K' = 2\omega + 4n - 1.$$

At this stage in the formulation of the problem, all the boundary conditions on the surface of the fluid sphere (except the condition of continuity of the normal components of the stress for the terms corresponding to an index $n > 2$) are satisfied by the hydrodynamic field given by the relations (3.11) and (3.12). So the available coefficients A_j must satisfy only the remaining boundary conditions (i) on the tube wall and (ii) far from the drop.

But with the selected frame, the no-slip condition on the tube wall cannot be strictly expressed by means of a finite number of terms of the series expansions (3.11) and, in addition, these expansions cannot represent the real flow in the whole domain (i.e. inside the infinitely long tube) because they imply infinite velocities for $r \to \infty$.

From now on we shall use a special technique (Bourot 1969; Coutanceau & Thizon 1978) based upon three proposals.

First proposal. The experiment (figures 11 to 14) shows that, beyond a certain relatively short distance L from the equatorial plane, the influence of the drop becomes negligible,† and thus the real external boundary T of the flow (i.e. the wall of the infinitely long tube) is replaced by a physically equivalent boundary B entirely situated at a finite distance from the origin: namely a part of the lateral surface of the tube completed by two perpendicular cross-sections situated at this axial distance L. The distance L is a function of the sphere-to-tube radius ratio λ and of the *a priori* fixed accuracy in this estimation of the perturbation in terms of velocity: thus it may be considered that the perturbations of the free stream below $0{\cdot}001U_0$ are physically

† In the moving reference frame the velocities take again approximately the unit value of the free stream, whereas in a fixed frame the fluid is practically at rest.

negligible, so that the two terminal cross-sections of the boundary B may be placed at the distance L corresponding to this approximation and consequently, on the boundary B, the non-dimensional velocity may be taken equal to unity (figure 1*b*).

Second proposal. The coefficients A_j are determined 'optimally' by minimizing the integral (evaluated on B) of the quadratic deviation between the imposed boundary data and the values provided by the trial functions given by the relations (3.11) and (3.12). Hence, imposing on B the velocity equal to the unit free-stream velocity, we must have

$$(U_{r_e})_{\text{imposed}} = t \quad \text{and} \quad (U_{\theta_e})_{\text{imposed}} = -s,$$

and according to the relations (3.11) the trial velocity components are

$$(U_{r_e})_{\text{trial}} = -\sum_{j=1,2,\ldots}^{\infty} A_j FA_j(r,t),$$

$$(U_{\theta_e})_{\text{trial}} = \sum_{j=1,2,\ldots}^{\infty} A_j FB_j(r,t).$$

So the integral is written as

$$I = \int_\Gamma [(-\sum_j A_j FA_j - t)^2 + (\sum_j A_j FB_j + s)^2]\, ds, \tag{3.13}$$

where Γ represents the outline of the meridian section of B (i.e. a rectangle, $2R_T$ in width and $2L$ in length, or, with lengths normalized by R, a rectangle: $2/\lambda$, $2L/R_T\lambda$) and ds a differential arc element of Γ. Then, the minimum of I corresponds to the following equations:

$$\frac{\partial I}{\partial A_i} = 0, \quad i = 1, 2, 3, \ldots, \infty.$$

From substituting in (3.13) the expression of FA and FB given by (3.12), we find that the coefficients A_j are solutions of the following symmetric linear system:

$$\sum_{j=1,2,\ldots}^{\infty} \int_\Gamma A_j(FA_i FA_j + FB_i FB_j)\, ds = -\int_\Gamma (tFA_i + sFB_i)\, ds, \quad i = 1, 2, \ldots, \infty. \tag{3.14}$$

Third proposal. For the numerical calculations, the series expansions are limited to a finite number N of terms and consequently the values of the summation indices i and j are also limited to N. The number N is chosen according to the tolerated deviation from the imposed boundary conditions.

3.1.2. *Numerical algorithms and parameters*

For the numerical calculations, the Gauss–Jordan elimination method has been used for solving the system of equations (3.14) and the integrals have been evaluated applying the Simpson algorithm. So, considering that the Gegenbauer polynomials are obtainable by a simple recurrence law, the programming was very easy: the various cases were treated changing the parameters λ, AL (representing the Γ rectangle elongation L/R_T) and N only.

In this way, the coefficients A_j have been determined for regularly spaced λ values ranging from zero (unbounded medium) to 0·8; accordingly AL was varying from 2 to 2·7 and N from 2 to 18. Now the coefficients are known all the hydrodynamic characteristics can be evaluated, e.g. velocity, stress, pressure and vorticity fields, and also the

drag wall correction factor Res: i.e. the ratio between the drags experienced by the drop in bounded and unbounded media respectively,

$$\text{Res} = Ps_\infty/Ps$$

if Ps_∞ represents the Poiseuille number for an unbounded medium, namely:

$$Ps_\infty = \frac{\omega+1}{2(6\omega+9)}.$$

On the other hand, as a test, it has been possible to estimate the precision with which the imposed boundary conditions have been satisfied effectively. In fact, it was found that the no-slip condition on the tube wall and the matching of the flow with the uniform velocity field in the two perpendicular cross-sections at a distance L from the equatorial plane have been satisfied with a very good precision, since in the most unfavourable calculated case ($\lambda = 0{\cdot}8$) the average of the deviation was less than 1% (for example, about 10^{-5} and 10^{-4} respectively for $\lambda = 0{\cdot}25$ and $\lambda = 0{\cdot}50$ with $N = 16$). Furthermore by increasing the value of N, it is possible to reduce this deviation notably. But, generally, 1% is a sufficient precision because the experimental results are not known with a better approximation. So, as it has also been previously shown by Bourot (1969) who proposed several useful types of application and then by Bourot & Sigli (1970) and Coutanceau (1971) who successfully calculated with the same technique other hydrodynamic fields in the domain of the Stokes simplification, this least-squares method appears to be very well adapted to treat these sorts of problems.

Remark. In this particular case, where the boundary conditions are given on two surfaces that are co-ordinate surfaces of two different frames (namely the spherical and cylindrical reference frames), it would have been possible to solve the problem using the technique proposed by Haberman & Sayre (1958). This consists in matching the two series expansions obtained (for the stream-function and velocity components) in the spherical and cylindrical co-ordinate frames respectively: the first satisfying exactly the condition on the sphere, the second the condition on the tube. But, as the number N of terms retained for the series in the calculations increases, the calculation development rapidly becomes complex. Moreover, as has been shown by Coutanceau (1968, 1971), the numerical results thus obtained represent the real flow in a satisfactory way only in the domain D' near the sphere (so the drag calculation is correct) but not in the whole 'useful' domain D (i.e. the whole domain perturbed by the sphere) and this more markedly as the sphere-to-tube radius ratio λ increases. On the other hand, it appeared that, with this technique proposed by Haberman & Sayre, increasing the term number N makes the flow representation more accurate in D' but does not extend this domain D'† and consequently does not permit any matching with the uniform flow. The authors do not mention this disadvantage.

So, the least-squares method appears to be not only more suitable because it gives more complete results but also because (and this is very important) it allows the calculation of two-dimensional or axisymmetric flows with obstacle and confining walls of various shapes (Bourot & Coutanceau 1971; Bourot 1975; Coutanceau & Dominguez 1979); it is not even necessary for numerical calculations to know the boundary

† In fact, we have shown (Coutanceau 1971) that the domain D' is practically represented by a sphere concentric with the spherical body and tangential to the tube in the equatorial plane; outside this domain D', the method proposed by Haberman & Sayre gives rise to singularities.

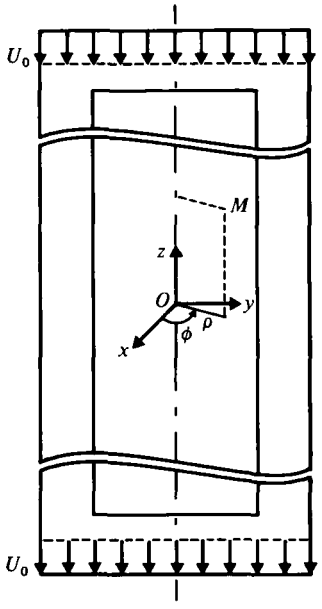

FIGURE 2. Cylindrical reference co-ordinate frame.

equations: point-by-point data are sufficient. However, the matrix of the system associated with the least-squares method tending to be ill-conditioned, the calculations must be done with sufficient precision (double precision).

When general solutions of the motion equations are not known in the form of series expansions analogous to the expressions (3.6) and (3.7) (for example, non-axisymmetric three-dimensional flows) the method 'of reflection' (Brenner & Happel 1958; Happel & Brenner 1965) can be used. But, in the case of a drop in a circular vertical tube, it is pointed out by experiment (Goldsmith & Mason 1963; Coutanceau & Thizon 1978*a*) that the drop itself adjusts its path along the tube axis and so the flow is always axisymmetric.

3.2. *The case of the cylindrical drop*

Now we suppose that the drop takes the shape of a cylinder closed at both ends, its length being very long compared with its radius R_E; the motion is then referred to a cylindrical co-ordinate system moving with the drop: ρ, ϕ, z (figure 2) and R_E and U_0 are considered as the length and velocity reference units respectively. Then we put

$$\lambda_E = \frac{R_E}{R_T}$$

and

$$Ps_E = \frac{\mu_e U_0}{4\Delta\rho g R_E^2}.$$

In this case, because of the particular form of the velocity field ($U_\rho = U_\phi = 0$) the stream function is not introduced and then the above boundary conditions (mentioned at the beginning of §3) are not sufficient to determine the problem; we complete them by imposing the continuity condition for the flows inside and outside

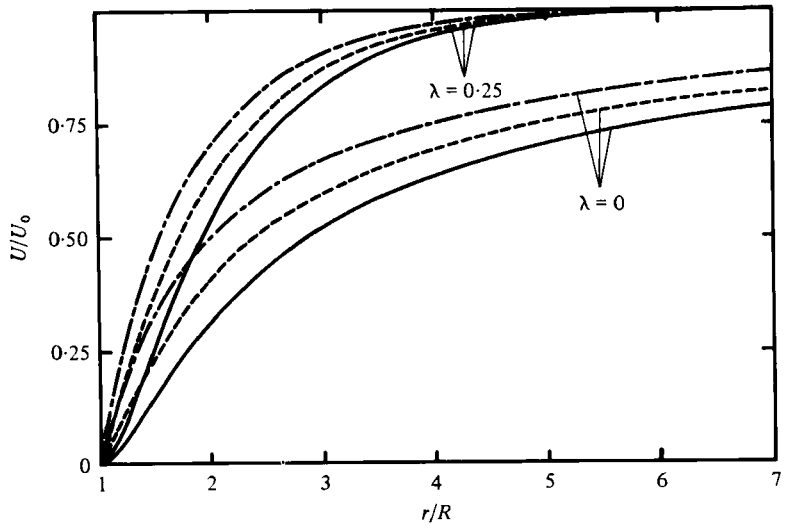

FIGURE 3. Velocity distribution along the exterior flow axis. Theoretical results for a spherical body when $\lambda = 0$ (indefinite medium) and $\lambda = 0{\cdot}25$; ——, $\omega = 0$; – – –, $\omega = 1$; — · —, $\omega \to \infty$.

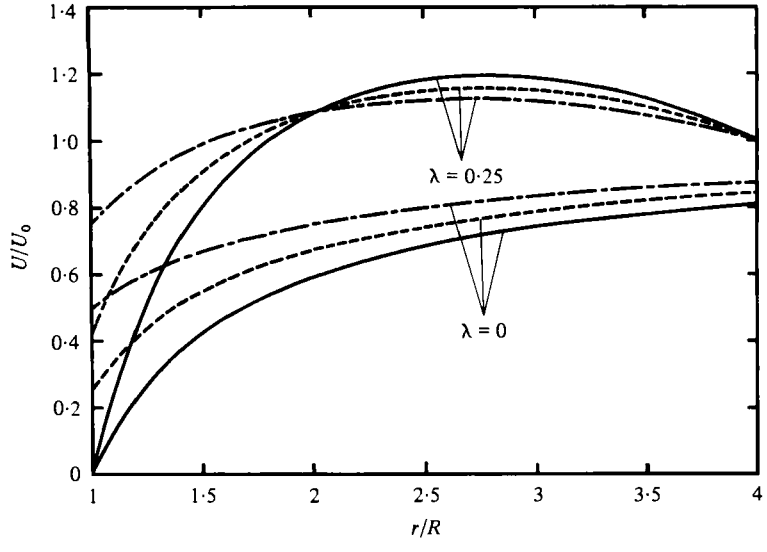

FIGURE 4. Velocity distribution in the equatorial plane of the exterior flow. Theoretical results for a spherical body when $\lambda = 0$ (indefinite medium) and $\lambda = 0{\cdot}25$: ——, $\omega = 0$; – – –, $\omega = 1$; — · —, $\omega \to \infty$.

the bubble respectively. So the flow rate must be, on the one hand, equal to zero across any perpendicular section of the drop:

$$q_{v_i} = 2\pi \int_0^1 U_{z_i}(\rho)\, \rho\, d\rho = 0$$

and, on the other hand, must be constant across any perpendicular cross-section of the

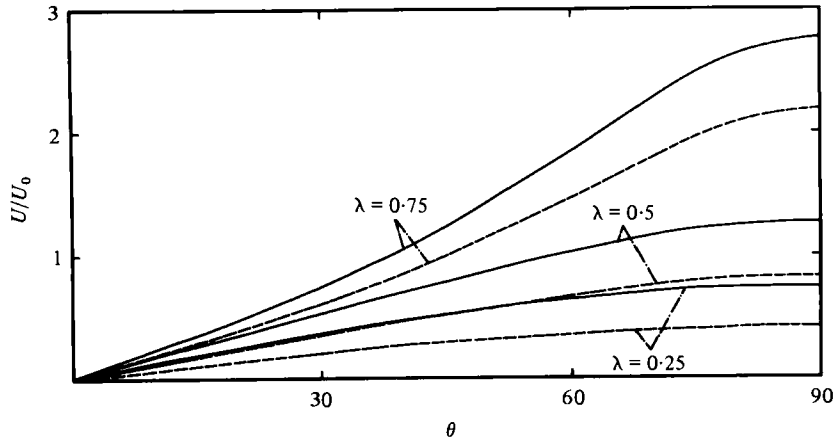

FIGURE 5. Velocity distribution on the body boundary. Theoretical results for a spherical body when $\lambda = 0{\cdot}25, 0{\cdot}50, 0{\cdot}75$: – – –, $\omega = 1$; ——, $\omega \to \infty$.

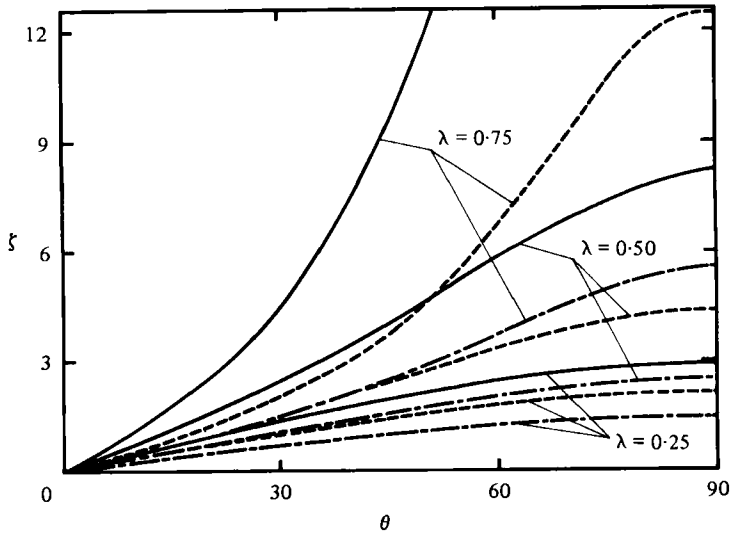

FIGURE 6. Vorticity distribution on the body boundary. Theoretical results for a spherical body when $\lambda = 0{\cdot}25.\ 0{\cdot}50,\ 0{\cdot}75$. ——, $\omega = 0$; – – –, $\omega = 1$; —·—, $\omega \to \infty$.

tube and equal to the flow rate of the unit uniform velocity field prevalent far from the drop:

$$q_{v_e} = 2\pi \int_0^{1/\lambda_E} U_{z_e}(\rho)\, \rho d\rho = \frac{\pi}{\lambda_E^2}.$$

The axial and tangential components of the velocity field that verify all these conditions are

$$U_{z_e}(\rho) = \frac{1}{DEN}\left(\left[\lambda_E^2(\lambda_E^2 - 1) - \frac{\lambda_E^4 \omega}{2}\right]\rho^2 + [1 + \lambda_E^4(\omega - 1)]\ln\rho + \lambda_E^2(1 - \lambda_E^2) + \omega\left(\frac{3\lambda_E^4}{4} - \frac{\lambda_E^2}{2} + \frac{1}{4}\right)\right],$$

$$U_{z_i}(\rho) = \frac{\omega}{DEN}\left[\left(\frac{1}{2} + \frac{\lambda_E^4}{2} - \lambda_E^2\right)\rho^2 - \left(\frac{1}{4} + \frac{\lambda_E^4}{4} - \frac{\lambda_E^2}{2}\right)\right],$$

with

$$DEN = \ln\frac{1}{\lambda_E}(\lambda_E^4\omega - \lambda_E^4 + 1) + \omega\left(\frac{3\lambda_E^4}{4} + \frac{1}{4} - \lambda_E^2\right) - (1-\lambda_E^2)^2,$$

and the terminal speed U_0 of the drop is given, in an non-dimensional form, by the Poiseuille number:

$$Ps_E = -\frac{DEN}{8(\lambda_E^4 - \lambda_E^4\omega - 1)}. \tag{3.15}$$

3.3. *Numerical results*

The main features (velocity, vorticity, pressure, streamlines, wall correction factor) of these two types of flows 'sphere-tube' and 'cylinder-tube' and their evolutions with λ have been completely calculated for three values of the viscosity ratio ω corresponding respectively to the cases of a bubble ($\omega \to \infty$), of a particular drop ($\omega = 1$) and of a rigid obstacle ($\omega = 0$) (Coutanceau 1971; Thizon 1977); as examples, figures 3 to 9 illustrate the main results.

Several interesting properties have been pointed out, in particular in the case of a spherical obstacle:

(*a*) For a given viscosity ratio ω, the extent of the domain disturbed by the sphere, evaluated in sphere radius R, becomes smaller as λ becomes greater (i.e. as the sphere is bigger compared with the tube) and, for a fixed value of λ, the sphere causes less disturbance in the external medium as ω is greater: the perturbation generated by a bubble is smaller than that generated by a solid sphere. For example, in the case when $\lambda = 0{\cdot}50$, on the flow axis and at a distance of one radius from the sphere, the relative velocity difference $(U_0 - U)/U_0$ is only 12 % for the bubble, 16 % for the drop and 24 % for the rigid sphere. At this same distance, for the bubble ($\omega \to \infty$), this relative difference with U_0 is 4 % for $\lambda = 0{\cdot}75$, 12 % for $\lambda = 0{\cdot}50$, 29 % for $\lambda = 0{\cdot}25$ and 50 % for $\lambda = 0$ (unbounded medium); it would be 69 % for $\omega = 0$ (rigid sphere) and $\lambda = 0$! The effect of concentration of the perturbation due to the wall presence is remarkable.

(*b*) In the case of fluid spheres, surface velocities exist that are increasing from the pole to the equator and that increase with λ and ω (see table 1). It is to be noticed that this equatorial surface velocity is relatively important compared with U_0 and that the difference between the spherical bubble and drop cases decreases when λ is increasing: its value is 44 % for $\lambda = 0{\cdot}25$, 33 % for $\lambda = 0{\cdot}50$ and 21 % for $\lambda = 0{\cdot}75$.

(*c*) The vorticity on the surface of the sphere increases as ω decreases and λ increases; in all cases, it is equal to zero on the pole and reaches a maximum at the equator. On the contrary with the surface velocity, the relative differences, corresponding to the variation with ω, increase as λ increases (table 2).

(*d*) The wall correction factor Res decreases notably when ω increases (table 3); consequently, the difference between the drags experienced by identical solid, liquid and gaseous spheres are exaggerated by the wall effect. So, for a spherical obstacle (with radius R) in an unbounded medium, the drag being given by

$$T_\infty = 6\pi\mu_e R U_0 \frac{2\mu_e + 3\mu_i}{3\mu_e + 3\mu_i}. \tag{3.16}$$

It is seen that keeping the other parameters constant the drag experienced by a spherical bubble is $\frac{2}{3}$ of the drag experienced by a rigid similar sphere; whereas, in

	$\lambda(= R/R_T)$			
$\omega(= \mu_e/\mu_i)$	0 unbounded medium	0·25	0·50	0·75
1 (drop)	$0{\cdot}25U_0$	$0{\cdot}42U_0$	$0{\cdot}84U_0$	$2{\cdot}19U_0$
∞ (bubble)	$0{\cdot}50U_0$	$0{\cdot}75U_0$	$1{\cdot}26U_0$	$2{\cdot}78U_0$

TABLE 1. Velocity on the equatorial circle of a spherical fluid body moving axially inside a tube.

	λ			
ω	0	0·25	0·50	0·75
0 (rigid)	1·50	2·94	8·02	39·45
1 (drop)	1·25	2·12	4·37	12·65
∞ (bubble)	1·00	1·50	2·53	5·56

TABLE 2. Vorticity on the equatorial circle of a spherical body moving axially inside a tube.

	λ		
ω	0·25	0·50	0·75
0 (rigid)	1·9796	5·950	40·7
1 (drop)	1·7315	4·120	20·3
∞ (bubble)	1·5398	3·223	16·2

TABLE 3. Wall correction factor Res for a spherical body moving axially inside a tube.

the case of a flow, confined when the sphere diameter is half the tube diameter ($\lambda = 0{\cdot}50$), the ratio between the corresponding drags (bubble and rigid sphere) is 0·36, so approximately $\frac{1}{3}$ only: then, for the same apparent weight, the bubble moves about 2·8 times more rapidly than the same rigid sphere!

Our theoretical values of Res are in very good agreement with those resulting from the application of the Haberman & Sayre technique and, also, with the simplified formula that these authors proposed, but, for the latter, the agreement is satisfactory only for values of λ smaller than 0·5. It must be noticed here that, for $\lambda > 0{\cdot}5$, this simplified formula of Haberman & Sayre gives values which are smaller than those given by the complete calculation and which deviate more and more when λ increases. So in the case of a solid sphere and for $\lambda = 0{\cdot}50$ and 0·75 this deviation is respectively 2% and 23%. Consequently, for solid spheres when $\lambda > 0{\cdot}5$, if great accuracy is required, the Haberman & Sayre simplified formula is not suitable. However, in the case of drops and bubbles, this formula represents the phenomenon in a slightly more satisfactory way than the exact calculation because, as we will show below, when the bubble loses its spherical shape, the drag that it experiences becomes effectively smaller: so, for a gas bubble and $\lambda = 0{\cdot}60$, the theoretical values obtained for Res are 5·20 and 5·12 using the exact calculation and the simplified formula respectively, whereas the measured value is 3·3; for $\lambda = 0{\cdot}75$ the values are, in the same order: 16·2, 14·4 and 4·7.

Finally, as has been mentioned in §3.1.1, it is interesting to evaluate, on the surface of the spherical bubble and drop, the relative importance of the difference between the

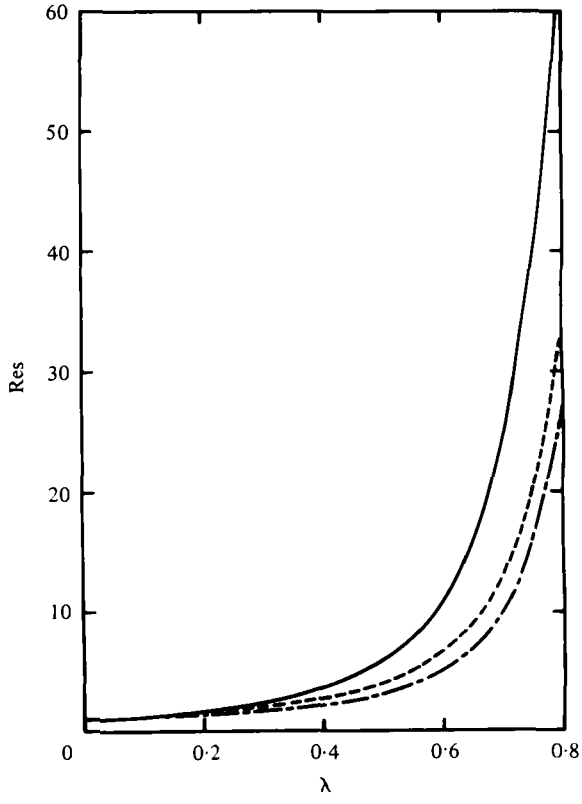

FIGURE 7. Wall correction factor Res in function of λ. Theoretical results for a spherical body: ——, $\omega = 0$; – – –, $\omega = 1$; — · —, $\omega \to \infty$.

external and internal radial components of the stress, corresponding to the terms of the series associated with $n > 2$, compared with the principal term $n = 2$. Indeed, it is to be remembered that the equality of these stress components cannot occur because of the *a priori* assumption of a spherical shape for the fluid body. We found that this stress difference equals zero at the equator and is a maximum at the pole; for $\omega \to \infty$ (and $\omega = 1$) the magnitude of this maximum is 2 % (2 %), 12 % (11 %), 26 % (24 %) respectively for $\lambda = 0{\cdot}25$, $0{\cdot}50$ and $0{\cdot}75$.

In the case of the cylindrical body, similar conclusions (to those drawn above) concerning the influence of the parameters λ_E and ω have been deduced; for example, figure 9 shows the velocity distribution in a cross-section for $\lambda = 0{\cdot}75$ in the cases of a bubble, a drop and a rigid cylinder. On the other hand, some comparisons have been established with the spherical bubble (figure 10).

4. Experimental study

It is now necessary to determine, by means of experiment, the respective ranges of λ where the theoretical results satisfactorily represent the real flow, i.e. the ranges of the λ values, where the wall effect on the shape of the fluid body is either negligible (spherical shape) or a maximum (cylindrical shape). Thus, we have undertaken this experimental study in the case of an air bubble, in order to determine the shape of the

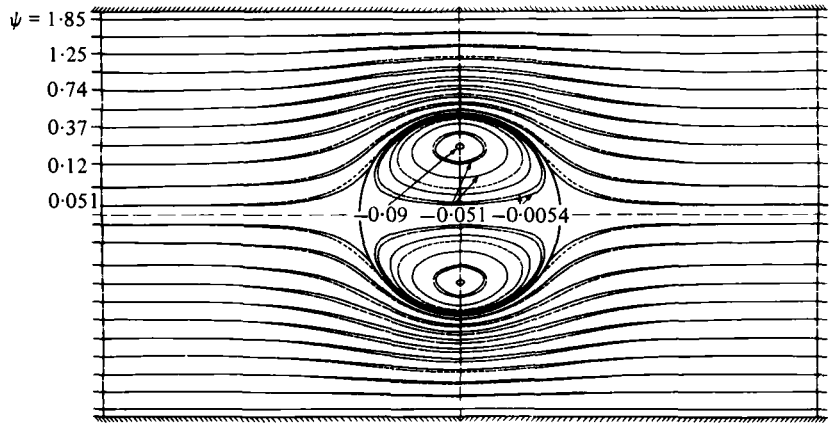

FIGURE 8. Streamline patterns of the exterior and interior flows. Theoretical results: – – –, spherical drop ($\omega = 1$); ——, bubble ($\omega \to \infty$). $\lambda = 0{\cdot}50$.

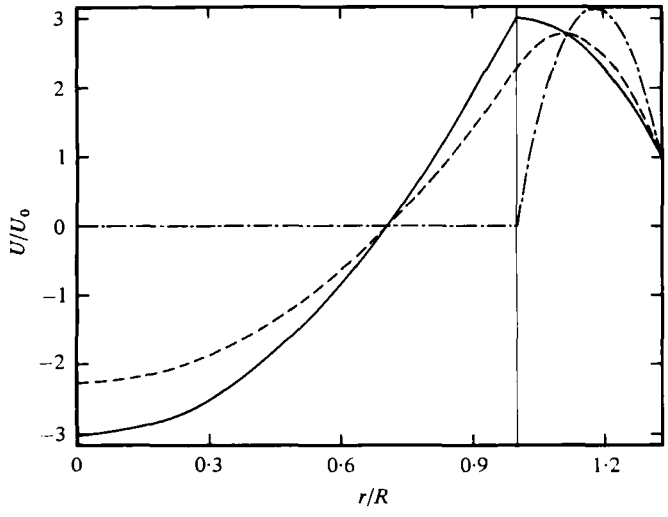

FIGURE 9. Velocity distribution in a right section interior and exterior to the body. Theoretical results for a cylindrical body when $\lambda = 0{\cdot}75$: ——, $\omega \to \infty$; – – –, $\omega = 1$; — · —, $\omega = 0$.

bubble, and also its rising speed, the domain disturbed by its presence, the hydrodynamic field it generates and the influence of the bubble-to-tube radius ratio λ on these characteristics.

4.1. *Some preliminary notations*

Since the bubble can be, as it will be seen, variously shaped, we introduce the following notations: λ stands for the 'equivalent' radius ratio, i.e. the ratio between the equivalent radius R of the bubble (radius of the sphere of the same volume) with the tube radius R_T;† λ_E stands for the 'equatorial' radius ratio, i.e. the ratio between the equatorial radius R_E of the bubble (the radius of its equatorial cross-section) with

† Hence λ can take values superior to unity; it tends towards infinity when the bubble volume is increasing infinitely.

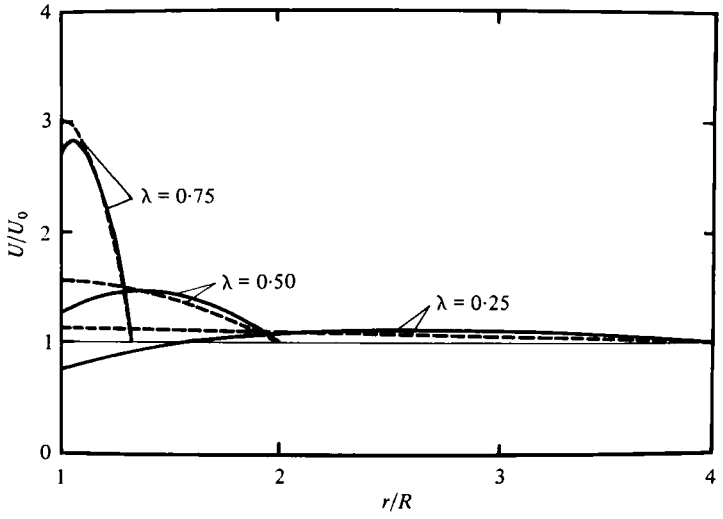

FIGURE 10. Velocity distribution in the equatorial plane of the exterior flow. Comparison between the theoretical results: ——, spherical bubble; – – –, cylindrical bubble.

the tube radius R_T; λ_A stands for the 'axial' radius ratio, i.e. the ratio between the 'axial radius' R_A of the bubble (i.e. the half-length of the bubble) with the tube radius R_T.

Except when it is differently specified, the dimensionless characteristic groups: Reynolds number, Morton number, Poiseuille number, etc., are defined with the 'equivalent' diameter d_e of the bubble.

4.2. *The experimental principle and the main elements of the apparatus*

A single air bubble rises freely along the axis of a transparent vertical circular tube whose length (120 cm) is great compared with its diameter so that the end perturbations are negligible. In order to obtain very low Reynolds numbers ($Re < 0{\cdot}20$) the tube is filled with a transparent liquid with a high viscosity: we used a silicone oil whose viscosity is about 300 P at 20 °C and whose surface tension amounts to 21 dynes/cm. The bubbles are produced with a piston moving in a jacket situated axially at the lower part of the tube; the air volume is determined by limiting the stroke of the piston with an adjustable stop. Reproducible results were obtained: the differences observed on the volumes of 40 bubbles were $< 2\,\%$. In addition, this air volume is accurately measured, by means of a sensitive flowmeter (based upon the translation of a soap film in a graduated tube) connected with the top end of the experiment tube, and so it has been possible to calibrate the system of bubble production and to observe the volume evolution during the rising of the bubble.

Visualization of the flow pattern was obtained by illuminating with a powerful arc-projector a thin (1 mm) meridian section of the tube after fine ($< 20\,\mu$m) bright particles of magnesium have been suspended uniformly in the liquid and by photographing the paths of these particles, in a perpendicular direction, when the bubble crosses the illuminated zone, i.e. about half-way up the tube. In order to compensate for the refraction effect, the tube is set in the axis of a square glass tank full of a transparent liquid, the refractive index of which is the same as that of the tested liquid.

Our apparatus allows two sorts of photographs: one with a fixed camera, the other with a camera moving in the same direction and with the same velocity as the bubble. In the latter, the camera is placed at the top of a vertical hydraulic jack and the motion is activated by a system of balance-weights and regularized by the flow of oil across narrow tubular holes drilled in the piston of the hydraulic jack. For the determination of the bubble boundary, a better definition is obtained with an illumination directed along and facing the optical axis of the camera.

The speed of ascent of the bubble is deduced from the indication provided by a pair of photocells, situated outside the tube in the lighted plane (10 cm distant one from the other) and connected to an electronic counter (the precision of which is 0·01 s): the crossing of the shadow cast by the bubble, in front of the photocells, is recorded by the counter. Subsequently, the speed of the camera is measured by another pair of photocells excited by an independent light and is adjusted to that of the bubble by means of the balance weights.

Regularly spaced values of the ratio λ, between the bubble equivalent radius and the tube radius, are obtained by experimenting with three tubes of different diameters (3, 4·4, 8·2 cm) and by varying the bubble volume. Our experiments are made with bubbles of greater volume than those used previously: the volume varies from about 1 to 40 cm^3. Thus, a large range of λ values is provided ($0{\cdot}15 \leqslant \lambda \leqslant 1{\cdot}17$) with suitable bubble sizes for a good visualization. Moreover, the overlapping of zones of λ resulting from the use of tubes of various diameters allowed us to verify the similarity of the phenomena.

We make sure that the terminal velocity of the bubble is reached when the photographs were taken so that the flow is steady in the moving reference frame.

During our experiments, we observe that the bubble path is rectilinear and axially centred; this fact has been previously mentioned by Goldsmith & Mason (1963).

All our experiments correspond to $Re \leqslant 0{\cdot}20$, $Mo \simeq 10^9$, $173 \leqslant Eo \leqslant 555$.

4.3. *Experimental results*

4.3.1. *General*

As examples three types of photographs are given. On one hand, for $\lambda = 0{\cdot}52$ and $\lambda = 0{\cdot}65$ the flow pattern is presented in a fixed frame (figures 11, 13) and in a moving frame (figures 12, 14); the white dashes are part of the trajectories described by the illuminated particles during the time of exposure. It appears that the flows are symmetrical about the equatorial plane; therefore, for the calculations the use of the Stokes simplification is justified.

'Viewed' in a fixed frame, the bubble appears to be 'accompanied' by a pattern of closed streamlines and the domain disturbed by its passage is clearly visible, but, since flow is unsteady, it is too difficult to deduce information about the velocity field. In the moving frame, however, when the synchronization of the rising speeds of the camera and of the bubble is good (this is effectively verified on figures 12, 14), the bubble is at rest and the flow is steady, and so it is possible to determine the velocities to good accuracy by measuring the lengths of the dashes; the special technique used for this measurement has been previously described by Coutanceau & Bouard (1977).

On the other hand, figure 15 shows (for $\lambda = 1{\cdot}17$) a bubble illuminated by a light facing the camera so that the inconvenient reflections on the bubble air–oil interface are eliminated and then it is easier to determine its shape precisely, but, the

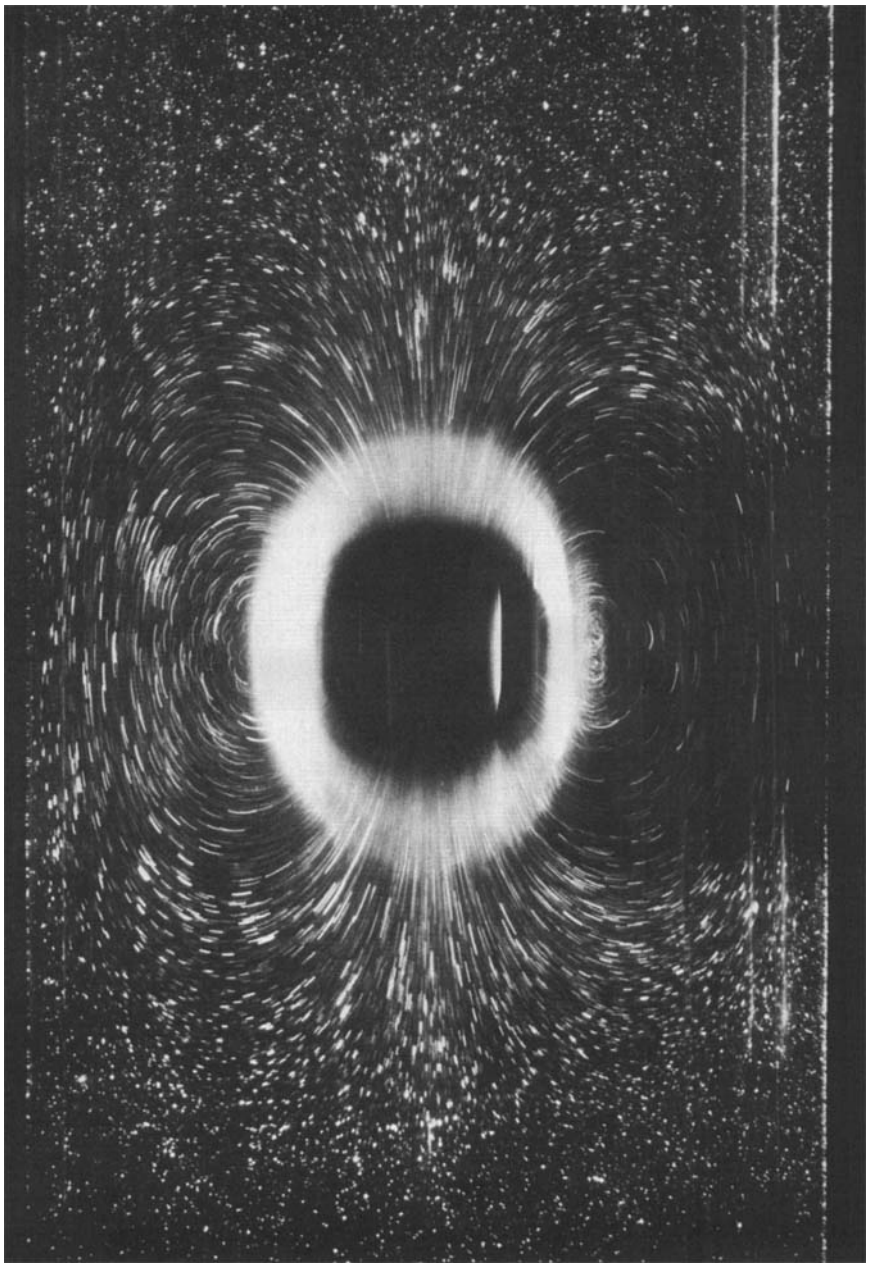

FIGURE 11. Flow visualization of a bubble rising axially in a tube when $\lambda = 0{\cdot}52$ (with a fixed camera).

visualization particles are no longer visible. In the case of this large bubble (22·5 cm^3 in volume) in a small tube (3 cm in diameter) a slight asymmetry exists analogous to that noticed by Goldsmith & Mason (1962): the base is somewhat flattened. This is probably due to the superficial tension phenomenon. However, in our experiments this asymmetry was always less than 1% and we did not take it into account.

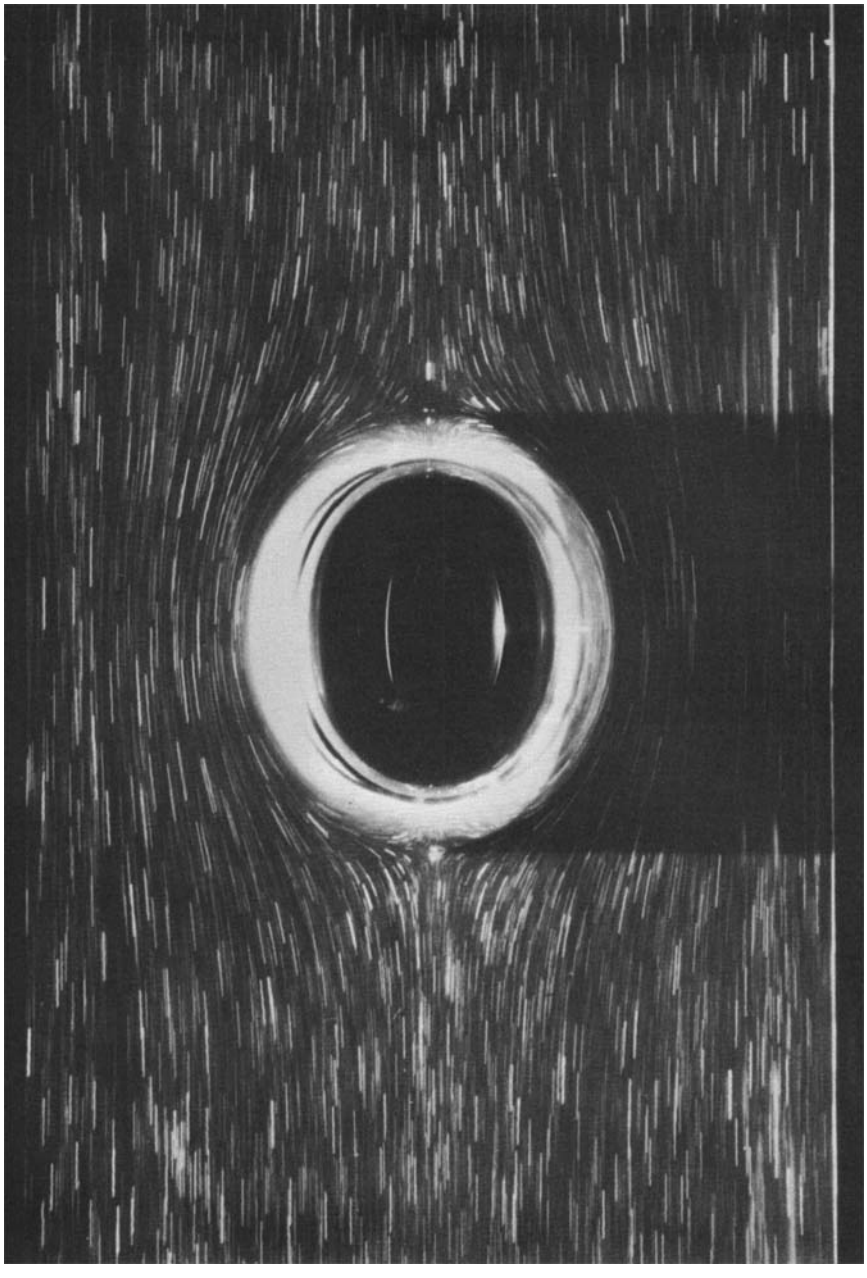

FIGURE 12. Flow visualization of a bubble rising axially in a tube when $\lambda = 0{\cdot}52$ (with a moving camera).

4.3.2. *Evolution of the air bubble shape in function of* λ (*figures* 11–17)

From our experiments it appears that the bubble retains a spherical shape (within an accuracy of 1%) for values of λ up to 0·20. But, for a given tube, the increase of the air volume causes a distortion of the bubble, which then progressively loses its spherical shape; at first its configuration can be considered to a good approximation as an

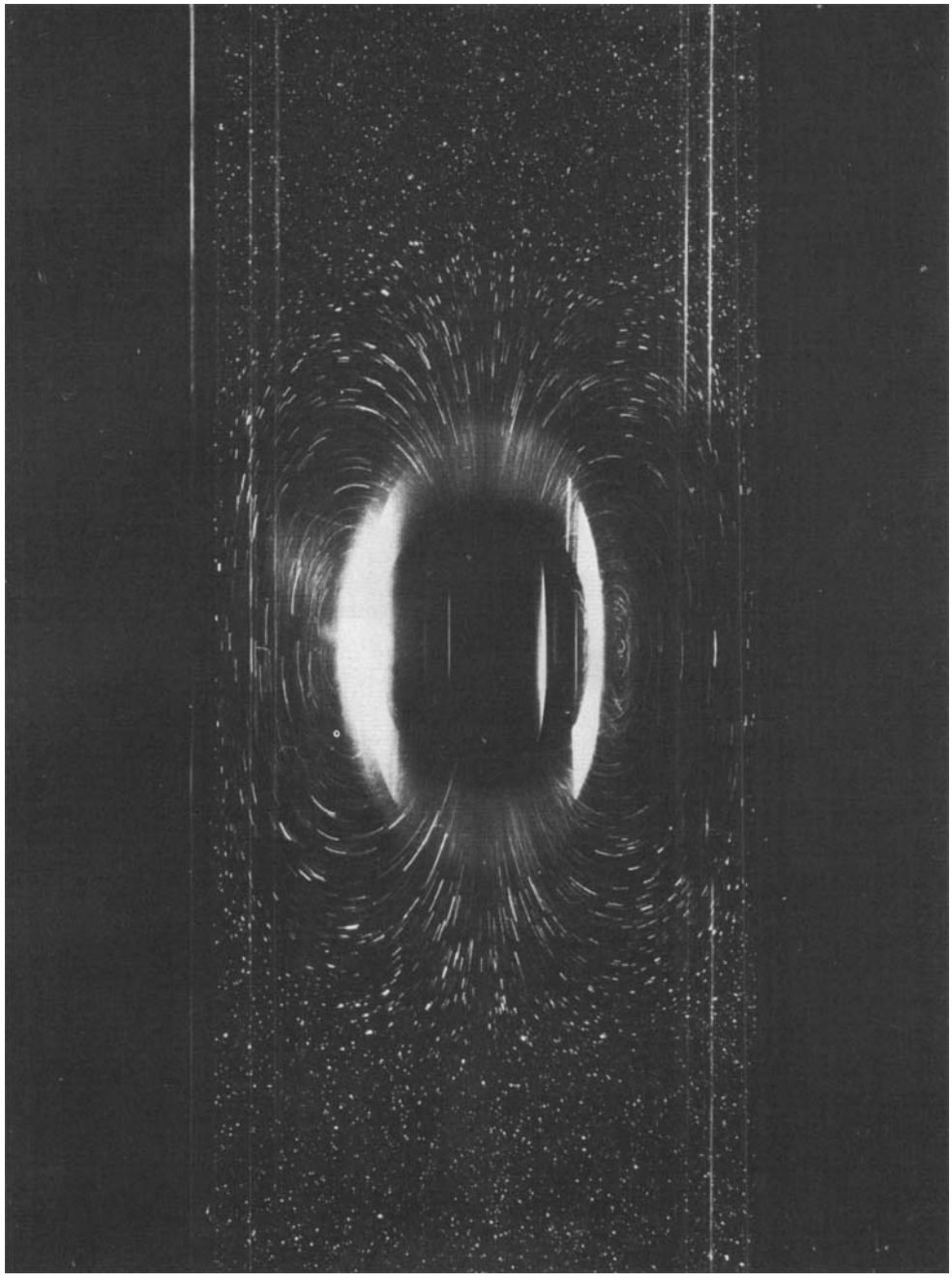

FIGURE 13. Flow visualization of a bubble rising axially in a tube when $\lambda = 0{\cdot}65$ (with a fixed camera).

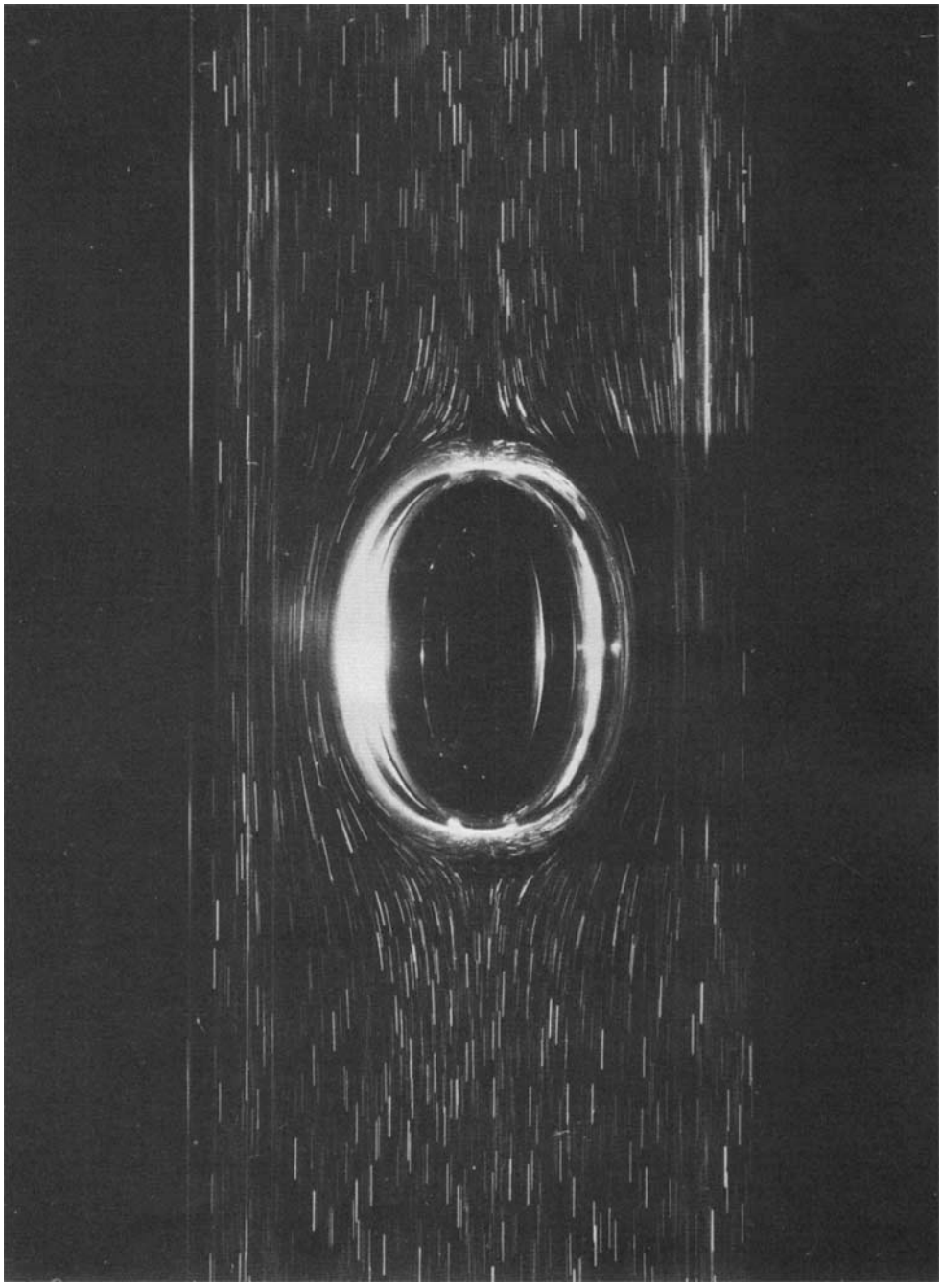

FIGURE 14. Flow visualization of a bubble rising axially in a tube when $\lambda = 0{\cdot}65$ (with a moving camera).

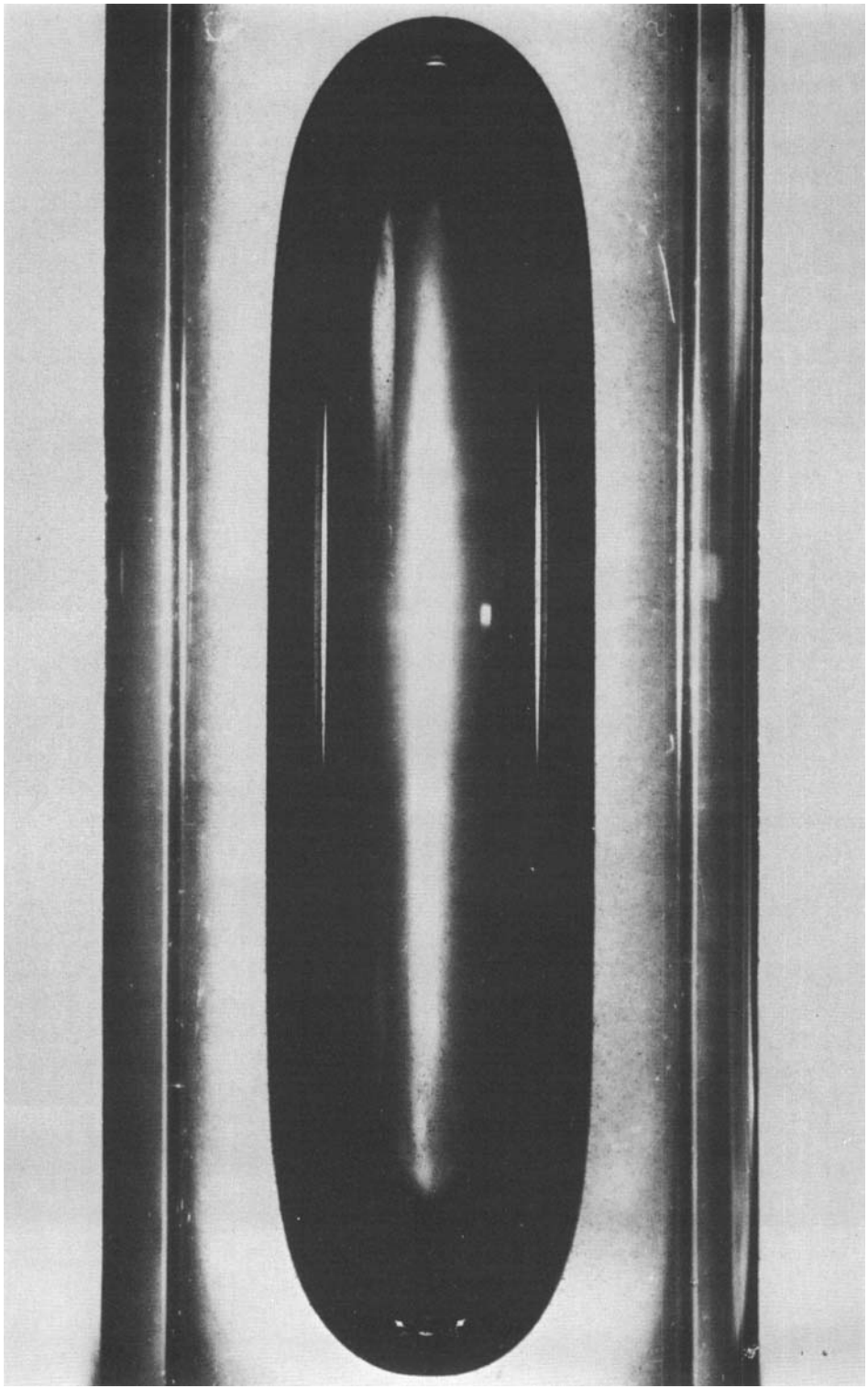

FIGURE 15. Visualization of the shape of a bubble rising axially in a tube when $\lambda = 1{\cdot}17$.

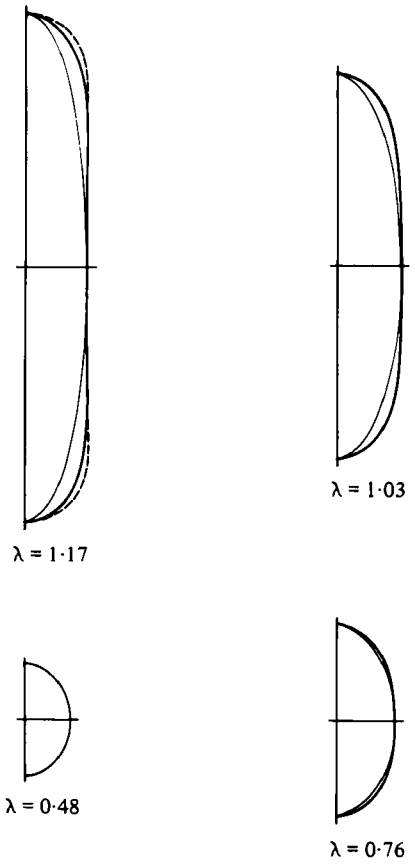

FIGURE 16. Evolution with λ of the shape of an air bubble: ——, real bubble; ——, ellipsoid with the same axis; – – –, cylindrical shape.

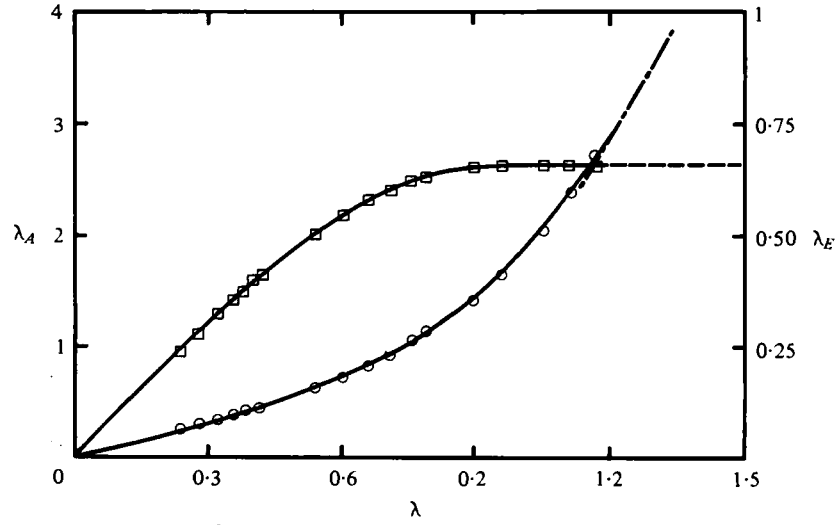

FIGURE 17. Evolution with λ of the equatorial and axial radius ratios of the real bubble. Experimental results: -□-, λ_E; -○-, λ_A. Limiting theoretical curves corresponding to a cylindrical bubble: – – –, $\lambda_{E\lim} = 0{\cdot}66$; — · —, $\lambda_{A\lim} = 1{\cdot}53\lambda^3 + 0{\cdot}22$.

ellipsoid whose large axis is parallel to the direction of the flow. This ellipsoidal shape is maintained (within 2 %) up to about $\lambda = 0{\cdot}60$. Beyond this value, the outline of the bubble differs more and more from that of the ellipsoidal shape and in the end it tends towards the cylindrical shape, being concentric with the tube and bounded approximately with two spherical caps at both ends. For the greatest value of λ used ($\lambda = 1{\cdot}17$) it was found that the maximum deviation between the real bubble shape and this schematic cylindrical one is localized at $\theta \simeq 15°$ (figure 16) and is limited to 7% only; even if the spherical caps were replaced by suitable spheroidal caps, the approximation would be almost perfect.

In order to characterize the bubble deformation we consider (in figure 17) the evolution of λ_E and λ_A; we remember that they represent respectively the ratios of the equatorial and axial radii of the bubble with the tube radius.

It is seen that, for $\lambda \leqslant 0{\cdot}20$, the evolutions are linear, but, when λ is increasing, i.e., for a given tube, the bubble volume is increasing, the increase in equatorial radius of the bubble becomes smaller as the increase in axial radius becomes larger. Moreover, as the bubble becomes more nearly cylindrical its rising speed as well as its equatorial radius tend towards the limits $U_{O1\lim}$ and $\lambda_{E1\lim}$ respectively; these two features were also observed by Goldsmith & Mason (1962) and Zukoski (1966) for bubbles and by Ho & Leal (1975) for drops. We found that, for the air–silicone-oil system, the limit $\lambda_{E1\lim}$ is reached practically (within 1%) when $\lambda = 1$; $\lambda_{E1\lim} = 0{\cdot}66$. This value is in good agreement with that (0·667) given by the empirical formula proposed by Zukoski where the surface tension is taken into account. It also agrees with the theoretical relation (3.15) for the cylindrical air bubble in which Ps_E is calculated using our measured value $U_{O1\lim}$ and the surface tension is not taken into account. It appears that for $\lambda > 1$ the bubble behaves dynamically as a cylindrical bubble and that in our experiments the surface-tension effects remain negligible (less than 1%) even in the more favourable cases.

For $\lambda = 1{\cdot}17$ the experimental 'axial radius' is also found to be the same (within 1·5 %) as the axial radius $\lambda_{A1\lim}$ of the cylindrical bubble of the same volume having the terminal velocity $U_{O1\lim}$ (and therefore an equatorial radius equal to 0·66) and, schematically, bounded by two spherical caps. Consequently, from about $\lambda = 1{\cdot}15$, he shape of the real bubble can be represented, to a good approximation, by $\lambda_{E1\lim} = 0{\cdot}66$ and $\lambda_{A1\lim} = 1{\cdot}53\lambda^3 + 0{\cdot}22$.

Using a technique of least-squares curve fitting, we have represented the outline of the meridian section of the bubble with an equation, for any value of λ, in the form

$$r(t) = 1 + \sum_{n=0,2,4,\ldots}^{N} \alpha_n(\lambda) P_n(t), \tag{4.1}$$

where r represents the non-dimensional polar radius normalized with the equatorial radius R_E, t the cosine of the colatitude θ and P_n the Legendre polynomial of degree n. Taking into account the symmetry of the bubble about the equatorial plane, only the even values of n are to be retained. The coefficients α_n and the equatorial radius R_E are expressed in terms of λ by means of analogous developments; then we put

$$\alpha_n(th\,\lambda) = \sum_{i=1,3,5,\ldots}^{N} \beta_{n,i} P_i(th\lambda), \tag{4.2}$$

$$\lambda_E(th\,\lambda) = R_E/R_T = \sum_{i=1,3,5,\ldots}^{N} \chi_i P_i(th\,\lambda). \tag{4.3}$$

i	α_0	α_2	α_4	α_6	α_8	λ_E	Ω
1	0·408570 E+00	0·123522 E+01	0·913285 E+00	0·747324 E+00	0·662235 E+00	0·845515 E+00	0·114982 E+01
3	0·255358 E+00	0·984506 E+00	0·111846 E+01	0·110565 E+01	0·108000 E+01	−0·190974 E+00	−0·174592 E+00
5	−0·623237 E−01	−0·406442 E−02	0·404611 E+00	0·640840 E+00	0·767890 E+00	−0·297553 E−01	0·469587 E−02
7	−0·351996 E−01	−0·185014 E+00	−0·190207 E+00	−0·538907 E−01	0·672670 E−01	0·383854 E−01	0·187490 E−01
9	0·125721 E−01	−0·490941 E−01	−0·248816 E+00	−0·355625 E+00	−0·400307 E+00	−0·317122 E−02	0·132425 E−02
11	−0·474197 E−02	−0·216617 E−01	−0·901525 E−01	−0·234197 E+00	−0·357726 E+00		
13	−0·633884 E−02	−0·148475 E−01	0·182824 E−01	−0·304747 E−02	−0·384658 E−01		
15	0·328649 E−02	−0·114128 E−02	0·492477 E−01	0·100446 E+00	0·161045 E+00		
17	0·389599 E−02	0·142437 E−01	0·213599 E−01	0·599673 E−01	0·103897 E+00		
19	0·745461 E−03	0·198716 E−01	−0·451074 E−02	0·998783 E−02	−0·187046 E−01		
21	−0·542898 E−02	−0·998254 E−02	−0·739667 E−02	−0·123098 E−01	−0·465171 E−01		
23	0·401656 E−03	−0·453958 E−02	0·386895 E−02	−0·109732 E−01	0·159596 E−01		

TABLE 4. Coefficients $\beta_{n,i}$ (n = 0, 2, 4, 6, 8), χ_i, γ_i of the expansions (4.2), (4.3) and (4.6).

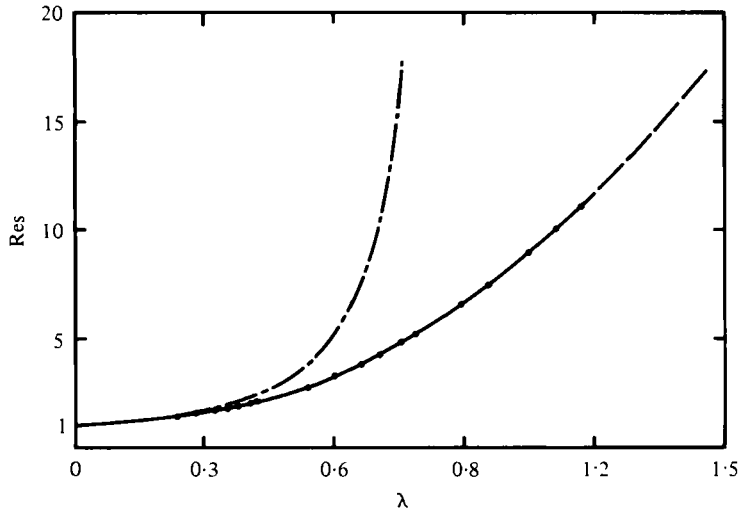

FIGURE 18. Wall correction factor Res in function of λ for a bubble rising axially in a tube: -●-, experimental results; – – –, limiting curve ($\mathrm{Res}_L = 8{\cdot}17\lambda^2$) corresponding to a cylindrical bubble; — · —, theoretical results for a spherical bubble.

The introduction of the variable $th\,\lambda$ allows us to represent the whole domain of λ including $\lambda = \infty$. It is then possible to take into account the corresponding limiting values of α_n and λ_E:†

$$\left.\begin{aligned} &\alpha_0(\infty) = \tfrac{1}{2}\pi - 1, \quad \alpha_n(\infty) = \frac{2n+1}{2}\pi\left[\frac{(n-1)!!}{n!!}\right]^2, \quad n = 2, 4, \ldots, \\ &\lambda_E(\infty) = 0{\cdot}66, \end{aligned}\right\} \tag{4.4}$$

where $(n-1)!! = 1\times 3\times 5\times \ldots \times (n-1)$, $n!! = 2\times 4\times 6\times \ldots \times n$.

The numerical values of the coefficients $\beta_{n,i}$ and χ_i have been determined by limiting the series expansions (4.1) and (4.3) to five terms and the series expansions (4.2) to 12 terms; these values are given in table 4.‡ In these conditions a satisfactory approximation is obtained: in all cases, the maximal deviation from the real bubble is situated at $\theta \simeq 10°$ and, for $\lambda \leqslant 1{\cdot}17$, it remains less than about 2%. As has been mentioned above, when $\lambda > 1{\cdot}17$ the bubble can be considered as a cylindrical bubble and then determined by $\lambda_{E\mathrm{lim}}$ and $\lambda_{A\mathrm{lim}}$. At this stage, if we know the injected air volume and the tube radius R_T (and consequently the equivalent radius R and the radius ratio λ), we can calculate the outline of the meridian section of the bubble for any value of λ.

4.3.3. *The drag wall correction factor*

It is to be remembered that the wall correction factor for the drag (Res) has been defined as the ratio between the drag T experienced by the bubble in the tube and the drag T_∞ experienced by a spherical bubble (having the same volume) in an unbounded medium:

$$\mathrm{Res} = T/T_\infty = U_{0\infty}/U_0,$$

† The limiting values of α_n and λ_E are determined from the fact that, when $\lambda \to \infty$, the bubble is an infinitely long cylinder whose radius normalized with the tube radius is $\lambda_{E\mathrm{lim}}$ and whose meridian boundary equation is $r = (1-t^2)^{-\frac{1}{2}}$.

‡ The limiting condition, for $\lambda \to \infty$, has been imposed and each coefficient of expansion depends slightly on the other coefficients.

where $U_{0\infty}$ represents the rising speed of the bubble in an unbounded medium. Hence

$$U_{0\infty} = \rho_e g R^2/3\mu_e.$$

The evolutions of the theoretical and experimental values of Res are given in figure 18: the two curves practically coincide up to $\lambda = 0{\cdot}20$ where the difference is of about 1% only; beyond this value they deviate increasingly as λ increases, the experimental curve always being below the theoretical one, so, with an equivalent volume, the real bubble takes a more profiled form and experiences a lower drag; its rising speed is all the more increased.

Consequently the deviation between the drags experienced by the real bubble and the solid sphere of equal volume is still greater than those mentioned in the theoretical analysis concerned with the spherical bubble. On the other hand, with the deduction of Haberman & Sayre (1958), it seems confirmed that the limiting value λ_L, corresponding to the beginning of the deviation between experimental and theoretical results, is smaller as the viscosity ratio ω is greater: then for $\omega = 13$ and 200 these authors found $\lambda_L = 0{\cdot}65$ and $0{\cdot}53$ respectively,† while for $\omega \to \infty$ (i.e. the gas bubble) we have already found a deviation of 5% for $\lambda = 0{\cdot}40$ and 20% for $\lambda = 0{\cdot}50$.

To represent the variation, with λ, of the coefficient Res, we propose the following empirical expression:

$$\text{Res} = \frac{1}{1 + \Omega(th\lambda)} \tag{4.5}$$

with

$$\Omega(th\lambda) = -\sum_{n=1,3,\ldots}^{N} \gamma_n P_n(th\lambda). \tag{4.6}$$

In the range $\lambda \leqslant 1{\cdot}17$, Res is obtained, within an accuracy better than 1%, by limiting (4.6) to five terms only (so $N = 9$); the corresponding values of the coefficients γ_n ($n = 1, 3, \ldots, 9$) are given in table 4.

Beyond this domain ($\lambda > 1{\cdot}17$) it is possible to use the relation appropriate to the cylindrical bubble whose radius normalized by the tube radius is λ_{Elim}; then we have

$$\text{Res} = 8\lambda^2/3\lambda_{Elim}^2\,[4\ln(1/\lambda_{Elim}) + 3 + (1/\lambda_{Elim}^4) - (4/\lambda_{Elim}^2)]. \tag{4.7}$$

Thus for the case where the superficial tension effects are negligible, when λ_{Elim} was found to equal $0{\cdot}66$, we obtain $\text{Res} = 8{\cdot}17\lambda^2$.

The matching of the curves corresponding to the two expressions (4.6) and (4.7) occurs for $\lambda \simeq 0{\cdot}9$ to within about 1% (figure 18). Thus an accurate calculation of Res (and consequently of the drag) is then possible in the whole domain $0 \leqslant \lambda \leqslant \infty$.

As we see it, the expression proposed by Uno & Kintner for Res is not suitable in the Hadamard regime; in the range of λ where it can be used, the corresponding data are 20–30% undervalued.

4.3.4. *Experimental velocity field. Comparison with the theoretical results*

The evolutions with λ of the experimental velocity along the flow axis and in the equatorial plane are given in figures 19 and 20; according to the curve, the distance r (evaluated from the origin) is normalized by either the axial or the equatorial bubble radius, R_A and R_E respectively. The following phenomena are verified:

† The authors did not give the exact value of the corresponding deviation between theoretical and experimental results, but from their graphics, it seems to be less than 10%.

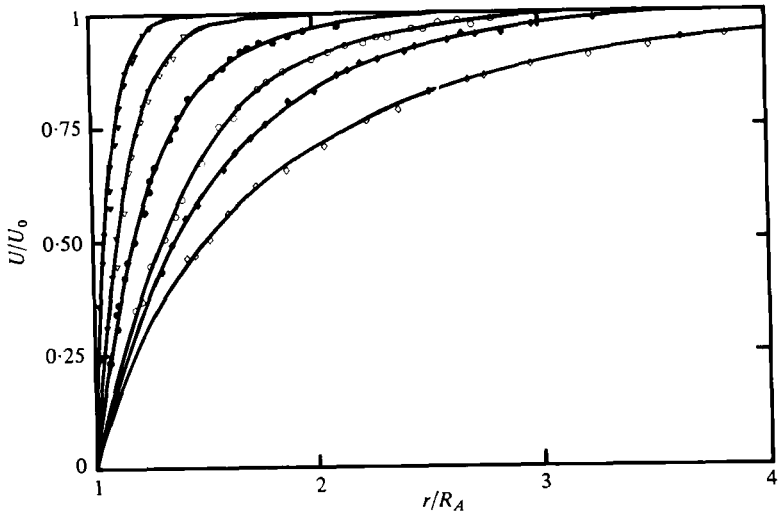

FIGURE 19. Evolution with λ of the velocity distribution along the exterior flow axis. Experimental results: -◇-, λ = 0·21; -◆-, λ = 0·39; -○-, λ = 0·48; -●-, λ = 0·68; -◁-, λ = 0·88; -▼-, λ = 1·3.

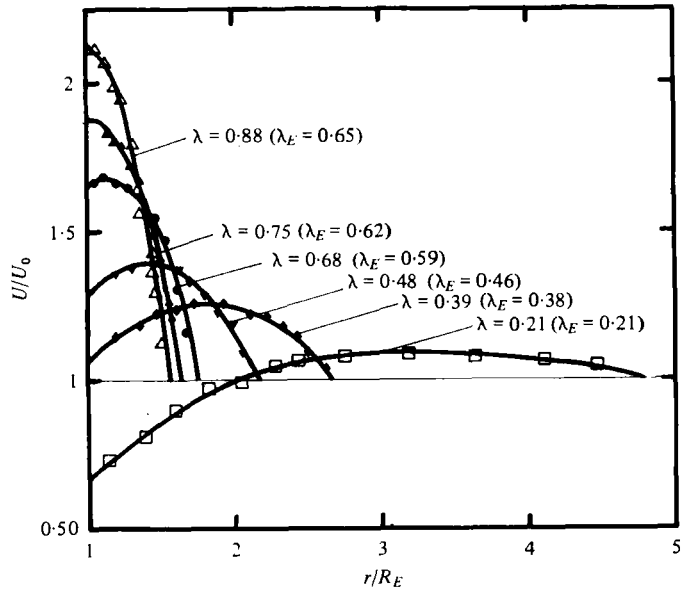

FIGURE 20. Evolution with λ of the velocity distribution in the exterior equatorial plane. Experimental results: -□-, λ = 0·21; -◆-, λ = 0·39; -▶-, λ = 0·48; -●-, λ = 0·68; -▲-, λ = 0·75; -△-, λ = 0·88.

(*a*) The length of the disturbed domain (along the axis) expressed with respect to R_A decreases as λ increases. For instance, the velocity again takes (within 1%) the unit value U_0 for the distances $3{\cdot}4R_A$, $2{\cdot}4R_A$ and $1{\cdot}9R_A$ respectively, for λ = 0·39, 0·68 and 0·88. In an unbounded region the comparable distance is $100R$! This result can be connected to the fact that flow disturbances die away exponentially along the

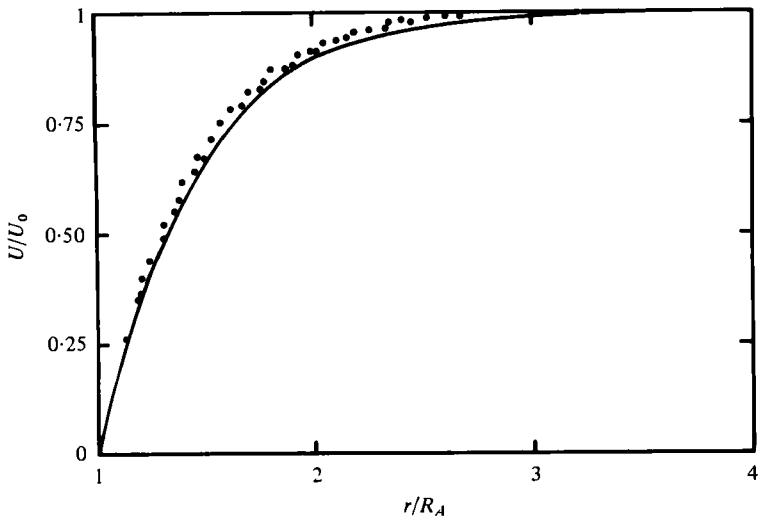

FIGURE 21. Velocity distribution along the exterior flow axis for $\lambda = 0\,48$ ($\lambda_A = 0{\cdot}54$). ——, theoretical results (spherical bubble); ●, experimental results.

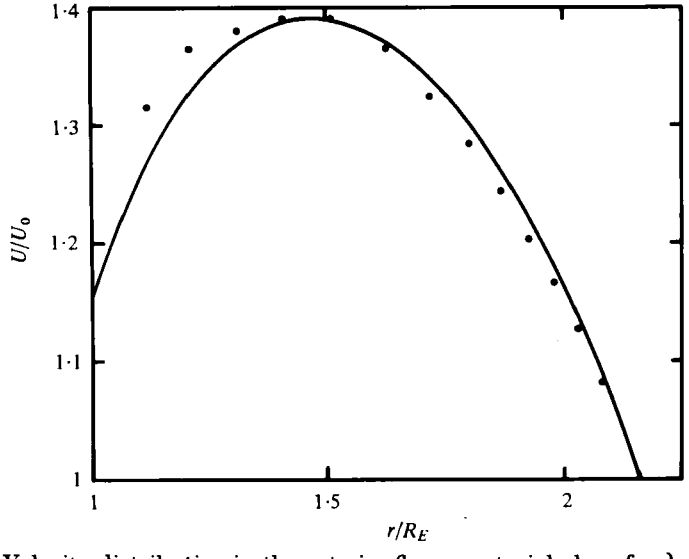

FIGURE 22. Velocity distribution in the exterior flow equatorial plane for $\lambda = 0{\cdot}48$ ($\lambda_E = 0{\cdot}46$). ——, theoretical results (spherical bubble); ●, experimental results.

tube. As we have mentioned, the calculation technique proposed in §3.1 is based upon this property.

(*b*) The relative velocities of the liquid particles in contact with the bubble surface are not equal to zero as in the case of a rigid body; the experimental results confirm the theoretical analysis: these surface velocities increase from the pole (stagnation point) to the equator; they also increase with wall proximity. These velocities can be important: for $\lambda > 0{\cdot}35$ they become greater, in the equatorial plane, than the terminal speed U_0 of the bubble. But these velocities are difficult to measure because of the reflections

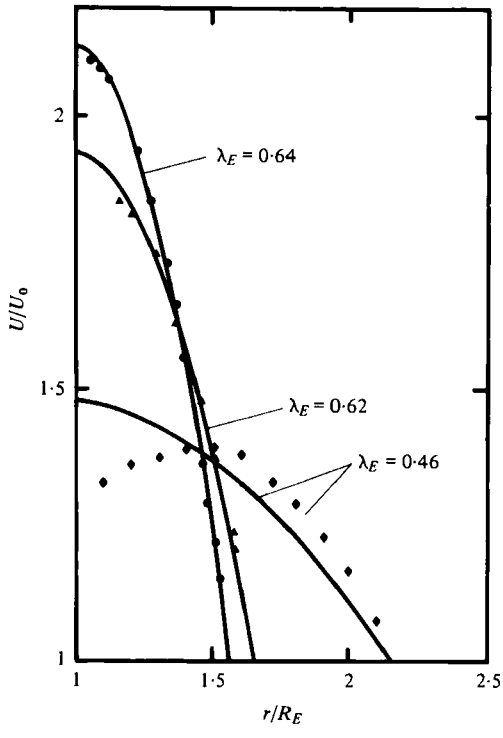

FIGURE 23. Evolution with λ of the velocity distribution in the exterior flow equatorial plane. ——, theoretical results (cylindrical bubble). Experimental results: ◆, $\lambda = 0{\cdot}48$ ($\lambda_E = 0{\cdot}46$); ▲, $\lambda = 0{\cdot}75$ ($\lambda_E = 0{\cdot}62$); ●, $\lambda = 0{\cdot}82$ ($\lambda_E = 0{\cdot}64$).

of light from the bubble surface and this effect becomes more important as the bubble size increases with respect to the tube diameter.

(*c*) In the equatorial plane, the curves present a maximum that becomes closer to the bubble as λ increases (figure 20); for the limiting case of a cylindrical bubble the velocity is a maximum on the bubble surface.

On the other hand, the comparison between our theoretical and experimental results points out that the experimental velocity fields are very well represented (better than 2%) by the calculated fields: for $\lambda \leqslant 0{\cdot}25$ with the spherical bubble model and for $\lambda \geqslant 0{\cdot}90$ (in the equatorial plane) with the cylindrical bubble model. This last remark agrees with the observations of Goldsmith & Mason (1962) which show a good correlation between the experiment and the cylindrical bubble hypothesis when the bubble length is at least twice the tube radius, i.e. in our case from $\lambda \simeq 1$. Unfortunately, when $\lambda < 1$ it is not possible to establish comparisons with other results because, to our knowledge, no similar investigation has been undertaken.

For $\lambda = 0{\cdot}48$ (i.e. $\lambda_E = 0{\cdot}46$ and $\lambda_A = 0{\cdot}54$), it is shown (figures 21 and 22) how the experimental velocities depart (4% in average only) from the theoretical results obtained for a spherical bubble whose radius corresponds to 0·54 for the velocity on the flow axis (figure 21) and to 0·46 for the velocity in the equatorial plane (figure 22). In particular, it is seen that the deformation of the real bubble involves an increasing of the axial and surface velocities.

Figure 23 presents the evolution with λ of the difference between the experimental

and theoretical velocity distributions outside the bubble in the equatorial plane of the flow when, in the calculations, the bubble is supposed cylindrical.

Finally, it is to be noticed that the experimental characteristics put in a non-dimensional form (shape of the bubble, velocity field, wall correction factor) are the same for equal values of λ, even if the experiments have been carried out in tubes of different diameters. In particular, all the data relative to the wall coefficient Res lie, plotted as a function of λ, on a single curve. Since Res is directly related to the Poiseuille number Ps (Res $= 1/12Ps$), it appears immediately that Ps is also a function of λ only. This remark confirms that, as was mentioned above, in our experiments the viscosity effects were dominant when compared with the inertial and superficial tension effects and so the Poiseuille number was effectively the characteristic group for similarity.

On the other hand, if the Poiseuille number is referred to the tube diameter, we find that it tends towards a limit (0·0100) when λ is increasing beyond unity. In our experiments relative to these cases, the Etvös number Eo (calculated with R_E) was about 4×10^2, so this limiting value is in good agreement with the constant value (0·0096) empirically proposed by White & Beardmore (1962) for $Eo > 70$.

5. Conclusion

The problem of the effects of the wall upon creeping flow induced by the translation of a fluid body along the axis of a vertical tube, filled with a quiescent and highly viscous liquid, has been considered both theoretically and experimentally.

The theoretical study allowed us, in particular, to establish some comparisons between the cases of rigid, liquid and gaseous spheres. Thus, it has been pointed out that the domain perturbed by the body (as has been defined above) is extending all the more as the body viscosity is higher: the domain perturbed by a gaseous bubble is less extended than the one perturbed by a solid sphere. On the other hand, the wall proximity causes a very strong concentration of the disturbance, for example, for a gaseous sphere (or a solid sphere) whose radius is half that of the tube radius, the axial dimension of the perturbed domain is 33 times (or 45 times) shorter than it would be in an unbounded medium. This concentration of the perturbation gives rise to an increase in the velocity gradients all around the body and then of the drag that the body experiences and this effect becomes larger as the body viscosity increases. Consequently the differences between the drags experienced by geometrically identical bodies resulting from their differing natures (solid, liquid or gaseous) are still exaggerated by the wall effect.

The experimental results, obtained in the case of an air bubble for $Re < 0{\cdot}2$, $Eo > 170$, $Mo \simeq 10^9$, confirm that, in these conditions, superficial velocities really exist on the bubble surface and are increased by the wall proximity. Furthermore, the way the bubble loses its spherical shape, when its size is increasing compared with the tube radius, has been described; from the empirical formulae that we proposed, it is possible to calculate this shape, as well as the terminal speed of the bubble, for the whole variation domain of the bubble-to-tube radius ratio λ, including the spherical and the cylindrical shapes. So it appears that the terminal speed is affected by the wall effect much sooner than the shape is, since for $\lambda = 0{\cdot}20$ when the bubble retains a good spherical shape its terminal speed is already 39 % less than the speed it would

have in an unbounded medium. In the Hadamard regime, for the wall effect to be reduced to 1% only, the minimal radius of the tube must be 150 times greater than the bubble radius!

Concerning the hydrodynamic field, the comparisons between theoretical and experimental results have shown a good agreement with the 'sphere–tube' flow (or 'cylinder–tube' flow) as far as the bubble retains effectively a spherical shape, i.e. for $\lambda < 0{\cdot}25$ (or when its becomes cylindrically shaped, for $\lambda > 1$). So it appears that the data given by our visualization technique were sufficiently accurate to allow us to perfect an efficient calculation method providing not only the drag coefficient but also the complete hydrodynamic field in the whole domain perturbed by the body. Later we hope that it will be possible to extend this method to calculate the flow around a real deformed bubble.

On the other hand, we shall continue the experimental work on drops and bubbles examining the respective influences of the inertial effects and of an eventual elasticity of the suspending liquid. An example of the first photographs that we obtain in this last case has been presented in the report of the Euromech Colloquium 98 (Van Vijngaarden & Vossers 1978).

The authors are grateful to Professor J.-M. Bourot, Director of the Fluid Mechanics Laboratory of Poitiers, for his useful suggestions. They also wish to thank R. Bouard, J.-R. Defaye, P. Falaise and G. Branger for their help respectively in drawing the graphs, translating this text into English and elaborating efficient experimental apparatus and techniques.

REFERENCES

Bourot, J. M. 1969 Sur l'application d'une méthode de moindres carrés à la résolution approchée du problème aux limites, pour certaines catégories d'écoulements. *J. Mec.* **8** (2), 301–322.

Bourot, J. M. 1975 Sur le calcul de l'écoulement irrotationnel et de l'écoulement de Stokes autour d'un obstacle de révolution de méridienne cardioïde; sur la structure du champ au voisinage du point de rebroussement. *C.r. Acad. Sci. Paris* A **281**, 179–182.

Bourot, J. M. & Sigli, D. 1970 Sur le calcul et l'étude expérimentale de l'écoulement de Stokes, autour d'une sphère progressant dans l'axe d'un cylindre quand le rapport des diamètres se rapproche de l'unité. *C.r. Acad. Sci. Paris* A **270**, 343–346.

Bourot, J. M. & Coutanceau, M. 1971 Sur le calcul numérique de l'écoulement de Stokes autour d'un obstacle de révolution dont la méridienne se rapproche d'un carré. *C.r. Acad. Sci. Paris* A **272**, 627–630.

Brenner, H. & Happel, J. 1958 Slow viscous flow past a sphere in a cylindrical tube. *J. Fluid Mech.* **4**, 195–213.

Collins, R. 1967 The effect of a containing cylindrical boundary on the velocity of a large gas bubble in a liquid. *J. Fluid Mech.* **28**, 97–112.

Coutanceau, M. 1968 Mouvement d'une sphère dans l'axe d'un cylindre contenant un liquide visqueux. *J. Mec.* **7** (1), 49–67.

Coutanceau, M. 1971 Contribution à l'étude théorique et expérimentale de l'écoulement autour d'une sphère qui se déplace dans l'axe d'un cylindre à faible nombre de Reynolds ou en régime irrotationnel. Thèse de Doctorat d'Etat, Poitiers.

Coutanceau, M. & Bouard, R. 1977 Experimental determination of the main features of the viscous flow in the wake of a circular cylinder in uniform translation. Part I. Steady flow. *J. Fluid Mech.* **79**, 231–256.

Coutanceau, M. & Thizon, P. 1978*a* Sur la détermination expérimentale des effets de paroi sur le comportement d'une bulle d'air en ascension dans un fluide visqueux. *C.r. Acad. Sci. Paris* B **287**, 93–96.

COUTANCEAU, M. & THIZON, P. 1978*b* Sur le calcul de l'écoulement engendré par la translation uniforme d'une goutte sphérique ou cylindrique suivant l'axe d'un tube vertical. *C.r. Acad. Sci. Paris* B **286**, 219–222.

COUTANCEAU, M. & DOMINGUEZ, H. 1979 Sur la détermination de l'influence d'un support sur l'écoulement autour d'un obstacle de révolution. (To appear.)

DAVIES, R. M. & TAYLOR, G. I. 1950 The mechanics of large bubbles rising through extended liquids and through liquids in tubes. *Proc. Roy. Soc.* A **200**, 375–390.

DUMITRESCU, D. T. 1943 Strömung an einer Luftblase im senkrechten Rohr. *Z. angew. Math. Mech.* **23**, 139–149.

GAL-OR, B., KLINZING, G. E. & TAVLARIDES, L. L. 1969 Bubble and drop phenomena. *Ind. Eng. Chem.* **61** (2), 21–34.

GOLDSMITH, H. L. & MASON, S. G. 1962 The movement of single large bubbles in closed vertical tubes. *J. Fluid Mech.* **14**, 42–58.

GOLDSMITH, H. L. & MASON, S. G. 1963 The flow of suspensions through tubes–II. Single large bubbles. *J. Colloid Sci.* **18**, 237–261.

GRACE, J. R. 1973 Shapes and velocities of bubbles rising in infinite liquids. *Trans. Inst. Chem. Eng.* **51**, 116–120.

GRACE, J. R., WAIREGI, T. & NGUYEN, T. H. 1976 Shapes and velocities of single drops and bubbles moving freely through immiscible liquids. *Trans. Inst. Chem. Eng.* **54**, 167–173.

HABERMAN, W. L. & SAYRE, R. M. 1958 Motion of rigid and fluid spheres in stationary and moving liquids inside cylindrical tubes. *David Taylor Model Basin Rep.* 1143.

HADAMARD, J. 1911 Mouvement permanent lent d'une sphère liquide et visqueuse dans un liquide visqueux. *C.r. Acad. Sci. Paris* **152**, 1735–1738.

HAPPEL, J. & BRENNER, H. 1965 *Low Reynolds Number Hydrodynamics*. Prentice-Hall.

HARPER, J. F. 1972 The motion of bubbles and drops through liquids. *Adv. Appl. Mech.* **12**, 59–130.

HETSRONI, G., HABER, S. & WACHOLDER, E. 1970 The flow fields in and around a droplet moving axially within a tube. *J. Fluid Mech.* **41**, 689–705.

HO, B. P. & LEAL, L. G. 1975 The creeping motion of liquid drops through a circular tube of comparable diameter. *J. Fluid Mech.* **71**, 361–383.

NICKLIN, D. J., WILKES, J. O. & DAVIDSON, J. F. 1962 Two phase flow in vertical tubes. *Trans. Inst. Chem. Eng.* **40**, 61–68.

RYBCZYŃSKI, W. 1911 Über die fortschreitende Bewegung einer flüssigen Kugel in einem zähen Medium. *Bull. Acad. Sci. Cracovie* A 40–46.

SAMPSON, R. A. 1891 On Stokes' current function. *Phil. Trans. Roy. Soc.* A **182**, 449–518.

SATAPATHY, R. & SMITH, W. 1961 The motion of single immiscible drops through a liquid. *J. Fluid Mech.* **10**, 561–570.

THIZON, P. 1977 Contribution à l'étude théorique et expérimentale des effets de parois sur le comportement de bulles en ascension dans un fluide visqueux. Thèse de Doctorat de troisième cycle, Poitiers.

TUNG, K. W. & PARLANGE, J. Y. 1976 Note on the motion of long bubbles in closed tubes. Influence of surface tension. *Acta Mech.* **24**, 313–317.

UNO, S. & KINTNER, R. C. 1956 Effect of wall proximity on the rate of rise of single air bubbles in a quiescent liquid. *A.I.Ch.E. J.* **2**, 420–425.

VAN WIJNGAARDEN, L. & VOSSERS, G. 1978 Mechanics and physics of gas bubbles in liquids: a report on Euromech 98. *J. Fluid Mech.* **87**, 695–704.

WALLIS, G. B. 1974 The terminal speed of single drops or bubbles in an infinite medium. *Int. J. Multiphase Flow* **1**, 491–511.

WHITE, E. T. & BEARDMORE, R. H. 1962 The velocity of rise of single cylindrical air bubbles through liquids contained in vertical tubes. *Chem. Eng. Sci.* **17**, 351–361.

ZUKOSKI, E. E. 1966 Influence of viscosity, surface tension, and inclination angle on motion of long bubbles in closed tubes. *J. Fluid Mech.* **25**, 821–837.